NUMERICAL SIMULATIONS OF TRANSONIC WINGTIP

by

SUPARAT CHANRITH

Presented to the Faculty of the Graduate School of

The University of Texas at Arlington in Partial Fulfillment

of the Requirements

for the Degree of

MASTER OF SCIENCE IN AEROSPACE ENGINEERING

THE UNIVERSITY OF TEXAS AT ARLINGTON

December 2013

This thesis is dedicated to my parents and all my teachers who gave me the opportunity to learn everything in my life.

Also, it is dedicated to all of my supporters who made me realize that education is truly important for a fulfilling life.

ACKNOWLEDGEMENTS

I would like to express my appreciation to all of my professors who gave me invaluable knowledge in aerospace engineering, especially Dr. Frank Lu, my supervising professor, who inspired and encouraged me throughout, giving me extensive guidance to proceed this thesis completely. I would also like to acknowledge Dr. Donald Wilson and Dr. Kamesh Subbarao for kindly serving on my committee. In addition, I would like to express my gratitude to the Royal Thai Air Force for providing me a scholarship to pursue my master degree. Morever, I would like to thank Wunnarat Rongrat, a former student, for his assistance in teaching me ANSYS FLUENT. Lastly, I wish to thank my parents and all of my friends for their help and support during this academic study.

November 13, 2013

ABSTRACT

NUMERICAL SIMULATIONS OF TRANSONIC WINGTIP

SUPARAT CHANRITH, M.S.

The University of Texas at Arlington, 2013

Supervising Professor: Dr. Frank K. Lu

This report presents numerical simulations using ANSYS FLUENT for a NACA 0012 wing both in two- and three-dimensional cases to compare with an experimental data. This comparison also allowed for any wall interference in wind tunnels to be examined. Moreover, the report also presents numerical simulation of a NACA 0012 wingtip. The simulations were conducted at Mach 0.5, 0.7, 0.75, and 0.8 at various chord Reynolds number and the angle of attack of 0, 2, 4, and 5°. The numerical and experimental data were in good agreement for the full wing and the wingtip cases.

TABLE OF CONTENTS

LIST OF ILLUSTRATIONS

LIST OF TABLES

CHAPTER 1

INTRODUCTION

1.1 Background

The transonic regime is a critical range of flight that has been widely studied from the 1930s. The vast majority of large air transports operate in this regime. Similarly, fighter and strike aircraft, despite being capable of supersonic flight, tend to operate in the transonic range. There are numerous factors that affect transonic flight such as shock wave and turbulent boundary-layer interaction which can induce flow separation and cause large-scale instabilities [1].

Experiments have been performed to investigate transonic airfoil and wing characteristics. Modern transonic wind tunnels that operate at high Reynolds numbers are able to obtain reasonably accurate data for large transports. Within the past two decades or so, advances in numerical techniques and computational power have ensured the viability of computational fluid dynamics (CFD) in studying fluid phenomena. An interesting development of late is the synergism between experimental and computational methods. For example, computations may be verified using existing experimental databases. On the other hand, computations have the ability to check experiments, such as to ensure that wall interference effects are properly taken into account.

Wall interference is particularly problematic in the transonic regime since shocks reflected off the walls can impinge on the model. Two strategies have been introduced to minimize wall interference: the test sections with ventilated walls and the test section with adaptive walls [2]. However, CFD can also be utilized to understand wall interference. Once a code is validated, a configuration can be numerically simulated with the tunnel walls in place or without, thereby providing data that can be used to examine the effect of the wall. In the preliminary stages of designing a test campaign, a proper model size for minimum interference can be obtained using CFD. A question that such a method raises is: why bother with experiment? In some situations and perhaps increasingly so, experiment may indeed be unnecessary. On the other hand, certain details may still be worthwhile to investigate via experiment, especially with complex flowfields. Examples include flow control where fine details may require extensive and costly computations.

1.2 Objectives

The present study applies a commercial flow solver ANSYS FLUENT to study the transonic flow over an airfoil and a wingtip both with a NACA 0012 profile. In the first case, the numerical simulation is used to determine if existing data [3] are free from wall interference. In the latter, the numerical results were compared with data from Werling [4]. The research objectives are to verify the experimental data and to confirm the ability of a commercial flow solver for simulating configurations in a transonic tunnel.

CHAPTER 2

NUMERICAL SIMULATIONS

The numerical approach utilized ANSYS Workbench. ANSYS DESIGN MODELER was used to created the two- and three-dimensional geometries, the latter including the four walls as in an actual wind tunnel. Subsequently, ANSYS MESHING was used to generate the unstructured meshes for using in the computations using ANSYS FLUENT and ANSYS CFD-Post.

2.1 Modeling

The model of this simulation is the NACA 0012 airfoil both in full- and half-wing. The computational domains created therefore match the test sections. In addition, the NACA 0012 airfoil had different chord lengths which were 1 m (39.37 in.), 0.0508 m (2 in.), and 0.635 m (25 in.). The first was used to understand the flow solver and did not represent an actual wing. But, the last two matched actual experiments. The three cases are:

- Case 1: A two-dimensional NACA 0012 airfoil wing which had a 1 m (39.37 in.) chord. A C-mesh domain as shown in Fig. 2.1 was created for defining the boundary conditions and creating the unstructured mesh. The radius of the C-mesh domain was 12.5 m (41 ft) and the rectangle was 12.5×25 m^2, as shown in the figure. The airfoil model was located in the middle of the C-mesh domain and was set only at zero incidence. This case was used to examine the ability of FLUENT for simulating transonic flow.

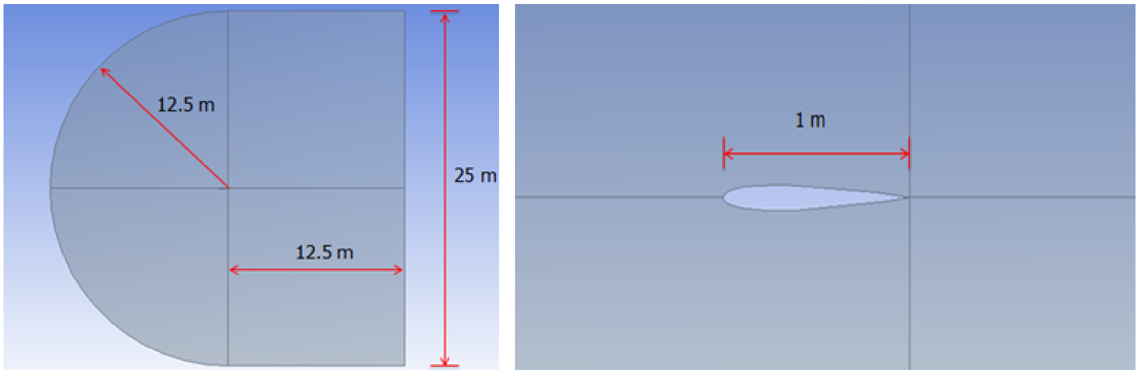

Figure 2.1 Case 1: Computational domain of two-dimensional model. The figure on the right is an enlargement showing the airfoil located ahead of the center of the semicircle in the figure on the left.

- Case 2: This three-dimensional full wing model had a 0.635 m (25 in.) chord length and 2.13 m (83.9 in) wing span that was located in the middle of a test section 2.2 m high by 2.13 m wide by 4.06 m long ($86.26 \times 83.9 \times 160$ in.). This case was used to simulate the experiments of [3]. The model was set at zero incidence as well.

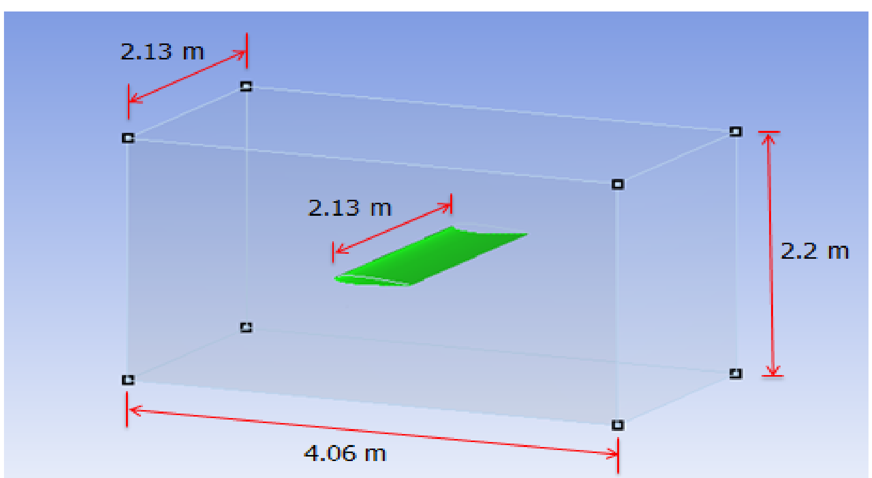

Figure 2.2 Case 2: Computational domain of three-dimensional full wing model.

- Case 3: A three-dimensional wing-tip model with a 0.0508 m (2 in.) chord length and 0.1092 m (4.3 in.) span. The model was located 0.292 m (11.5 in.) from the leading edge of a test section 0.186 m high, 0.232 m wide and 0.635 m long (7.75 × 9 × 25 in.). This case was used to simulate the experiments of [4] and the model was set only at zero incidence.

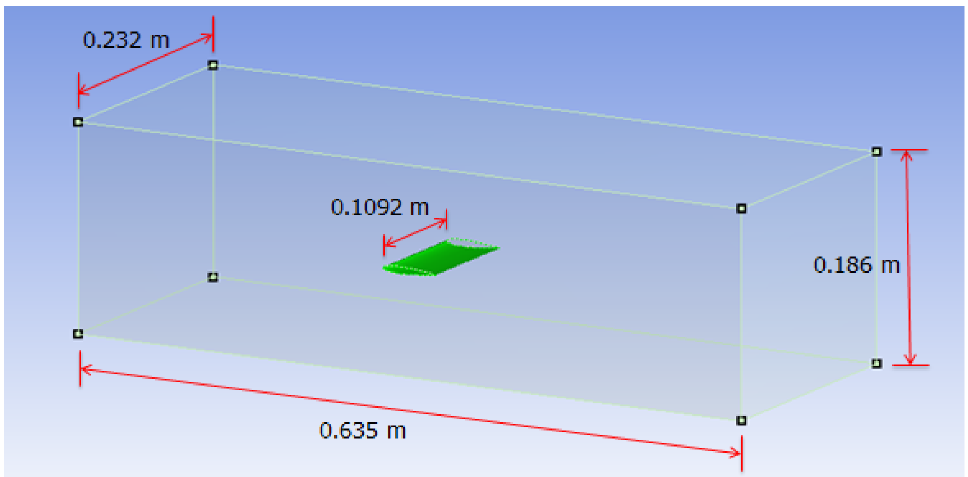

Figure 2.3 Case 3: Computational domain of three-dimensional half wing model.

2.2 Meshing

ANSYS MESHING was used to generate an unstructured mesh for the computations. The unstructured mesh consisted of small quadrilaterals or tetrahedrals near to areas of interest, namely, the wing, to larger sizes further away. This mesh distribution yielded accuracy and allows for complex gradients around the wing to be resolved for a minimum number of meshes. The final process of meshing is to define the boundary conditions for the model. Since the three-dimensional models were created within a test section, farfield boundary conditions were defined at the four walls. The airfoil model and the two sidewalls were assigned as wall boundary conditions.

Pressure boundary conditions were imposed on the top and bottom walls. These conditions were used to define the direction of air flow for accommodating changes in the angle of attack.

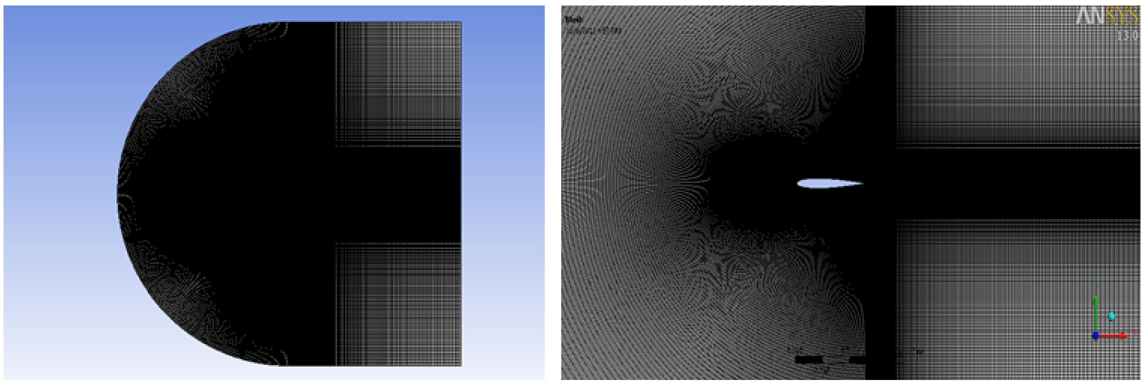

Figure 2.4 Mesh around a two-dimensional NACA 0012 airfoil.

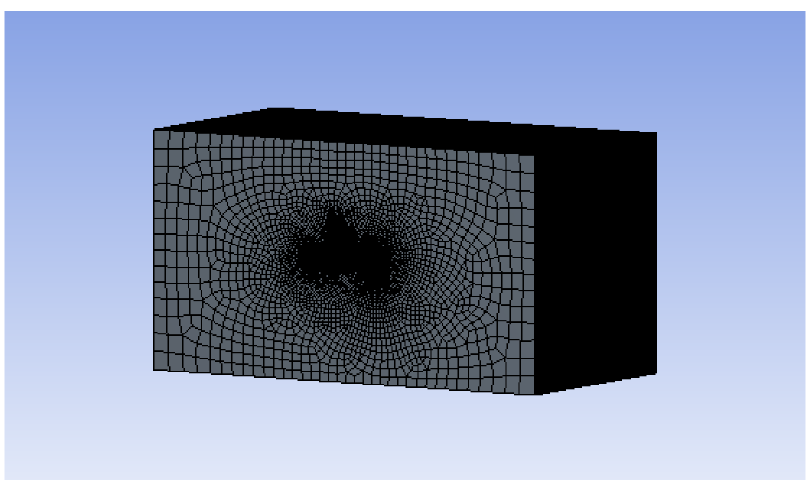

Figure 2.5 Mesh around a three-dimensional full-wing with a NACA 0012 profile.

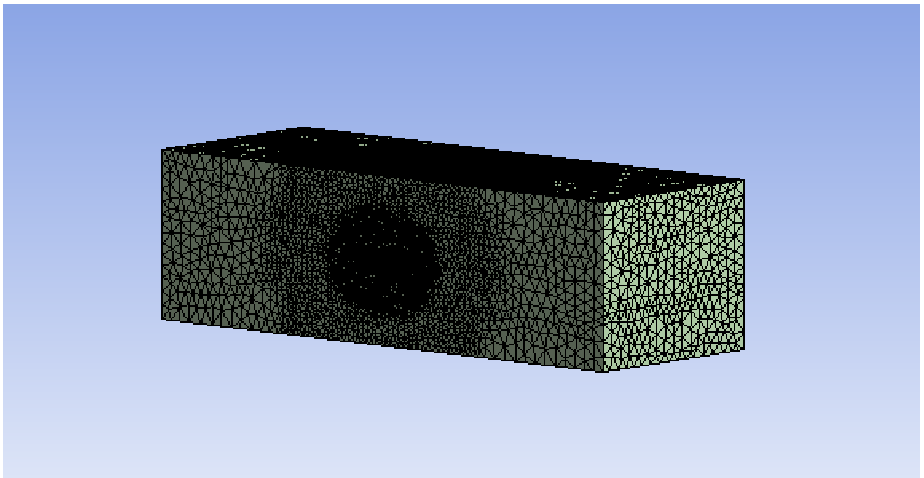

Figure 2.6 Mesh around a wingtip with a NACA 0012 profile.

Table 2.1 Meshing summary

Airfoil model	Meshing Method	Nodes	Elements
1 m chord (2-D)	Quadrilateral mesh	361,200	360,000
0.635 m chord (3-D)	Quadrilateral mesh	1,792,670	1,752,888
0.0508 m chord (3-D)	Tetrahedral mesh	378,552	2,070,661

2.3 Analysis

The flow solver is ANSYS FLUENT with density-based and steady options. The k-ω turbulence model with shear stress transport (SST) was used. This model has good behavior in examining the shock wave and pressure gradient [5] and thus it is suitable for our purpose. The simulations were conducted with an incoming Mach number of 0.5, 0.7, 0.75, and 0.8. The angle of attack was 0, 2, 4, and 5 deg and the Reynolds number based on the airfoil chord length as shown in Table 2.2. The free stream static pressure and temperature for the simulations were calculated using

$$P_\infty = P_0 \left[1 + \frac{(\gamma - 1)}{2} M_\infty^2 \right]^{(\gamma-1)/\gamma} \tag{2.1}$$

$$T_\infty = T_\circ \left[1 + \frac{(\gamma - 1)}{2} M_\infty^2 \right]^{-1} \tag{2.2}$$

The free-stream speed of sound and the free-stream velocity can be obtained by

$$a_\infty = \sqrt{\gamma R T_\infty} \tag{2.3}$$

$$V_\infty = a_\infty M_\infty \tag{2.4}$$

Sutherland's viscosity law for air was used for the viscosity of the flow and can be evaluated by

$$\mu(T) = \frac{1.458 \times 10^{-6} T^{3/2}}{T + 110.56} \tag{2.5}$$

Finally, the Reynolds number is calculated by

$$Re = \frac{\rho_\infty V_\infty}{\mu} \tag{2.6}$$

Table 2.2 Nominal Test Conditions

	Reynolds number		
Mach number	Case 1	Case 2	Case 3
0.50	9×10^6	6×10^6	-
0.70	12×10^6	8×10^6	-
0.75	-	-	6×10^5
0.80	13×10^6	8×10^6	-

CHAPTER 3

RESULTS AND DISCUSSION

The simulations for the flow over NACA 0012 both in two- and three-dimensions were compared to existing experimental data. The computed aerodynamic coefficients from the airfoil were compared with the experimental data of Mineck and Hartwich [3]. In this comparison, both infinite wing (two-dimensional) and finite wing with side walls were simulated, the latter being a rendition of the actual wind tunnel. For the finite wing, data at the mid-span were used for comparison with experiment. In addition, a set of lift and drag coefficients were obtained and compared with data from Werling [4].

3.1 Convergence

The simulations were defined to investigate the converged solution by monitoring the residuals of continuity, velocity components, energy, ω and k. Convergence criteria were determined when the residuals were less than 0.001. The maximum iteration was set to 2,000 in order to observe that the solution was converged, and the simulations automatically proceeded to the final step of iteration. In addition, lift and drag coefficients were monitored for examining the converged solution. The results are shown in Figs. 3.1–3.3. These figures show that convergence was achieved at about 800 iterations.

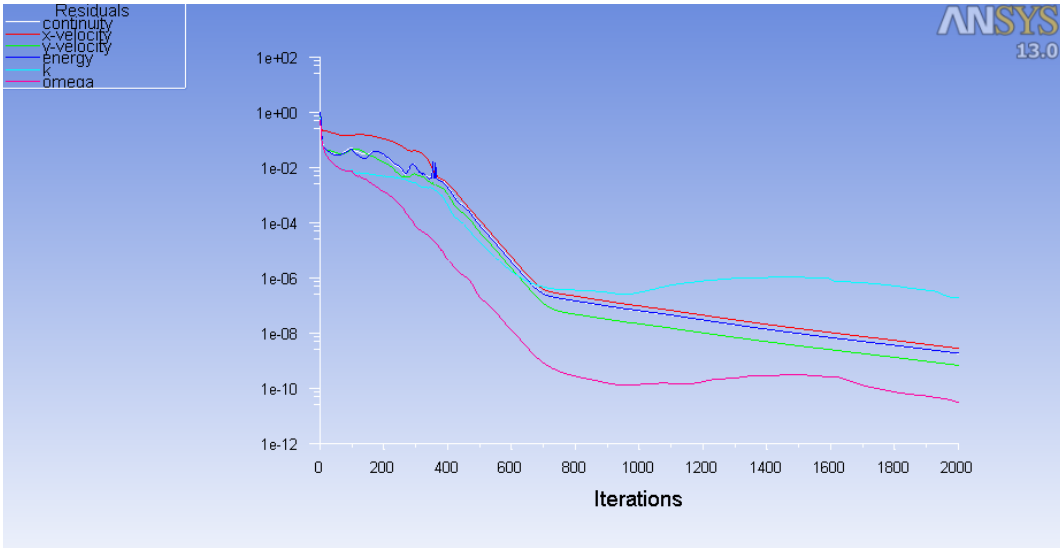

Figure 3.1 The iterations for the residual of continuity, velocity components, energy, ω and k at $M = 0.5$ and $\alpha = 5°$.

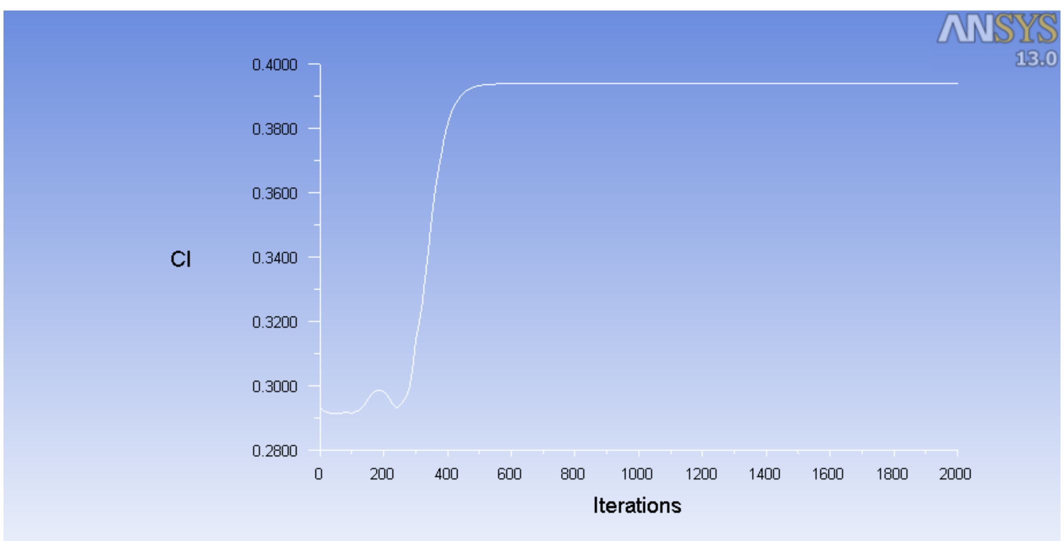

Figure 3.2 The iterations of lift convergence history at $M = 0.5$ and $\alpha = 5°$.

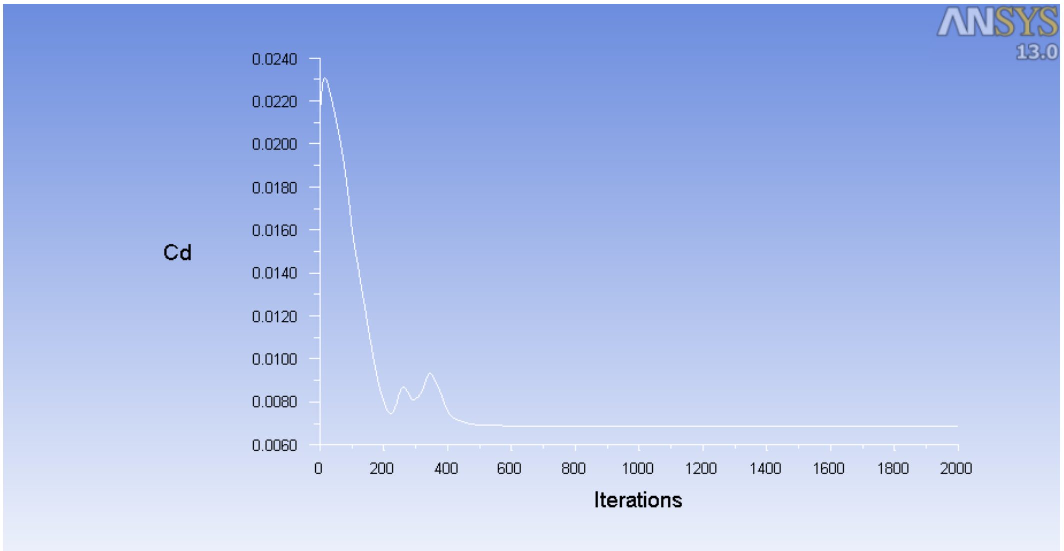

Figure 3.3 The iterations of drag convergence history at $M = 0.5$ and $\alpha = 5°$.

3.2 Results and Comparison

3.2.1 Pressure Distributions

Case 1: the numerical results of pressure distribution for the two-dimensional model with a 1 m chord length were plotted and compared with experimental data. The results agreed well with the experiment on both the upper and lower airfoil surfaces in the case of $M = 0.5$ and $\alpha = 0$, 2, 4, and 5°. For $M = 0.7$, the comparison showed good agreement only at $\alpha = 0$, whereas at $\alpha = 2$, 4, and 5°, the results showed small differences between numerical and experimental results. In the case of $M = 0.8$, also, only at $\alpha = 0$ presented a good comparison in pressure distribution. The results at $\alpha = 2$, 4, and 5° exhibited slight differences from the experimental data in the shock location.

Case 2: the numerical results of the three-dimensional model which has a 0.635 m (25 in.) chord length were plotted and compared with experimental data. The results presented a good agreement both on the upper and lower airfoil surfaces in the case of $M = 0.5$ at $\alpha = 0$, 2, 4, and 5°. Additionally, it can be observed that the experimental data is in between the two- and three-dimensional numerical results. At $\alpha = 0$, 2, 4, and 5° for $M = 0.7$ showed small differences in the distributions of pressure coefficient. Particularly, at $\alpha = 5°$, the shock position was slightly different from the experimental data and the two-dimensional simulation. At $M = 0.8$ and $\alpha = 0$, the pressure distribution exhibited good agreement with the two-dimensional simulation and with experiment, but the others presented distinct differences both on upper and lower surfaces, especially at the higher incidences of $\alpha = 4$ and 5°.

Case 3: the pressure coefficient distributions of the three-dimensional, wingtip model which has 0.0508 m (2 in.) chord length were obtained. This simulations were conducted only at $M = 0.75$ and $\alpha = 0$, 2, 4, and 5°. The pressure coefficients are shown in Figs. 3.22 and 3.23. For Case 3, the results produced non-uniform pressure distributions on the wing as shown in Figs. 3.24–3.27. Additionally, tunnel wall boundary-layer thickness was investigated in this case. Since these simulations were performed in the test section that had two sidewalls, the boundary-layer characteristics were determined. Fig. 3.29 showed the results of boundary-layer thickness in any distance from the wingtip model and its values were shown in Table 3.1.

Table 3.1 Tunnel Wall Boundary-Layer Thickness

Distance from wingtip model	Boundary-Layer Thickness (δ)
50 mm	5.824 mm
100 mm	8.532 mm
200 mm	6.690 mm
250 mm	11.905 mm

3.2.2 Lift and Drag Coefficients

The numerical lift and drag coefficients were compared with experimental data. The simulation was conducted at $M = 0.75$ and a chord Reynolds number of 6×10^5. The angle of attack was 0, 2, 4, and 5°. The results obtained from the simulation exhibited good agreement with the experimental data as shown in Fig. 3.30, but showing lower drag at $\alpha = 4$ and 5°.

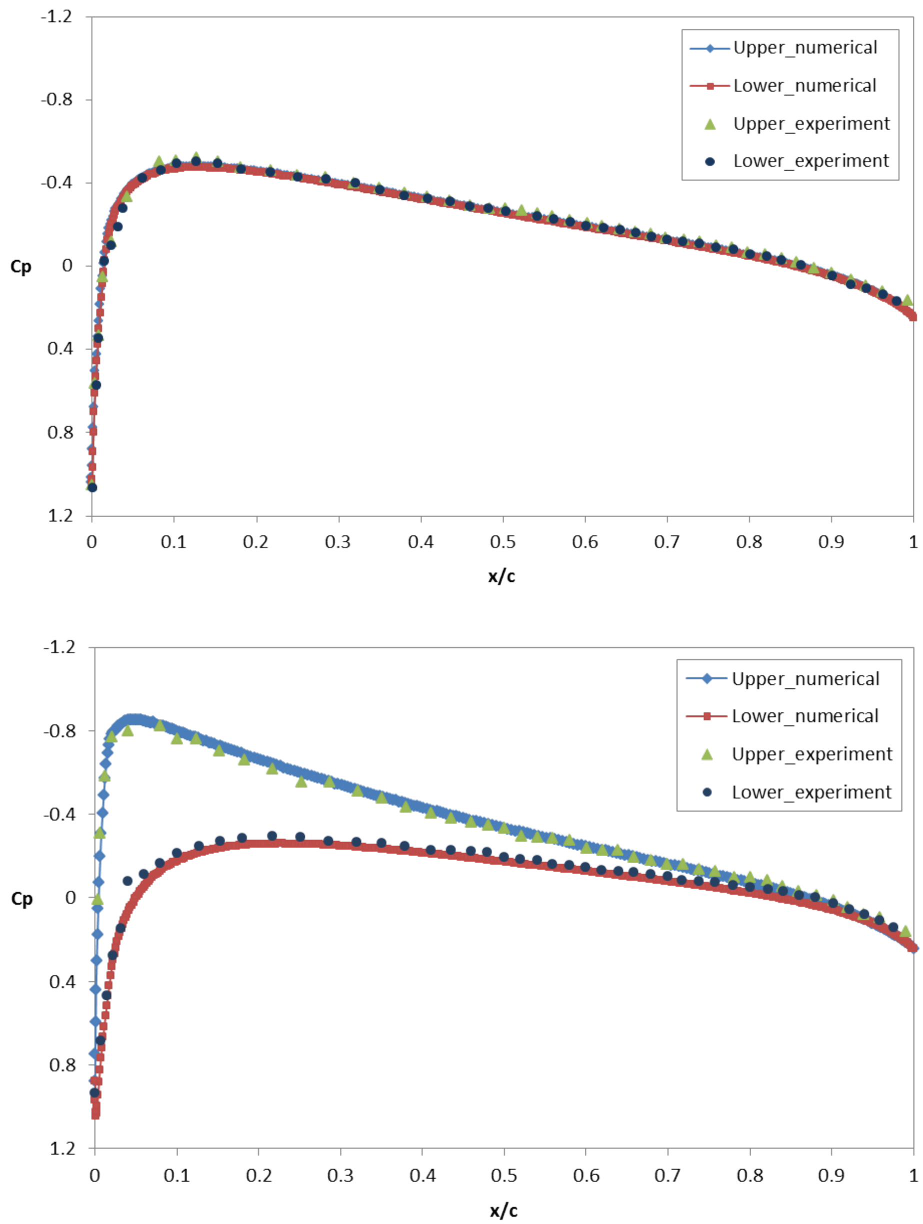

Figure 3.4 Case 1: Pressure coefficient distributions on NACA 0012 airfoil at $M = 0.5$, $R_c = 9 \times 10^6$, and $\alpha = 0$ and 2° respectively.

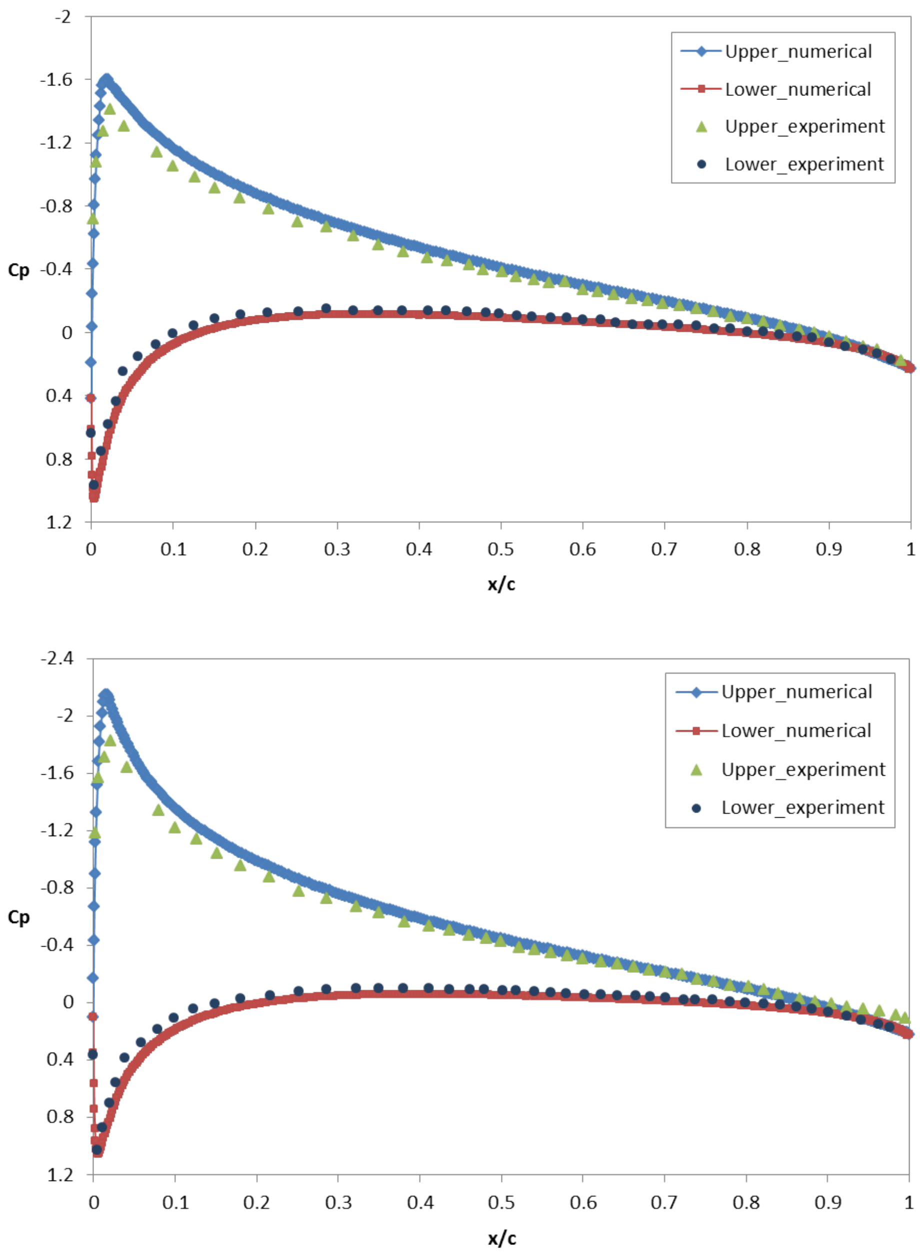

Figure 3.5 Case 1: Pressure coefficient distributions on NACA 0012 airfoil at $M = 0.5$, $R_c = 9 \times 10^6$, and $\alpha = 4$ and $5°$ respectively.

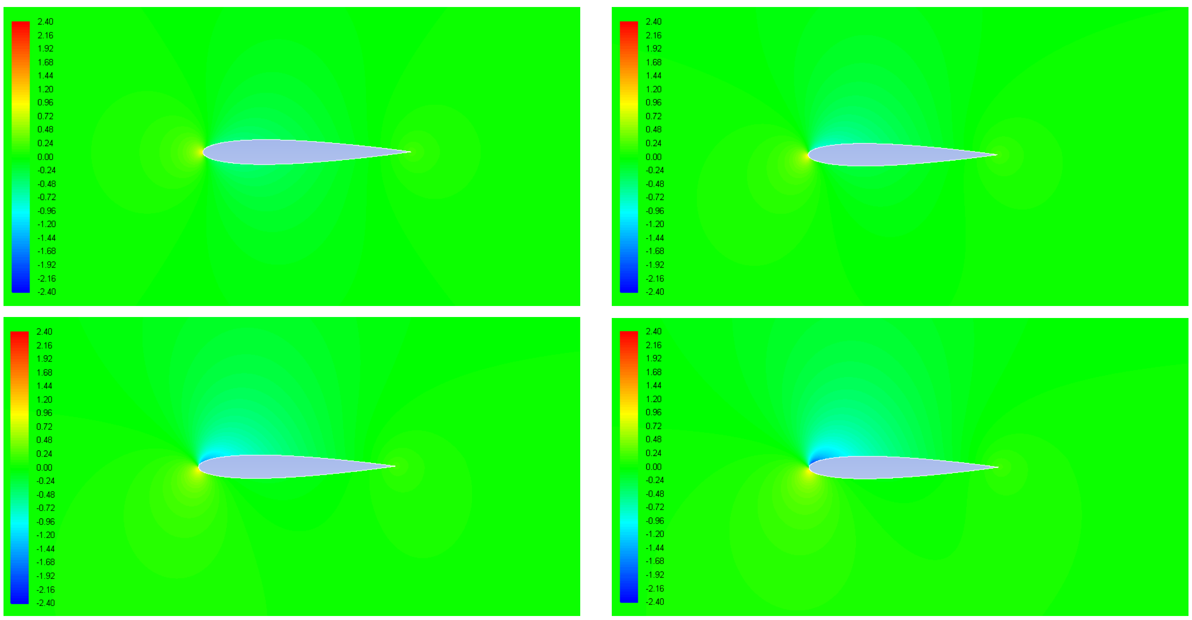

Figure 3.6 Case 1: Contour of pressure distributions on NACA 0012 airfoil at $M = 0.5$, $R_c = 9 \times 10^6$, and $\alpha = 0$, 2, 4, and 5° respectively.

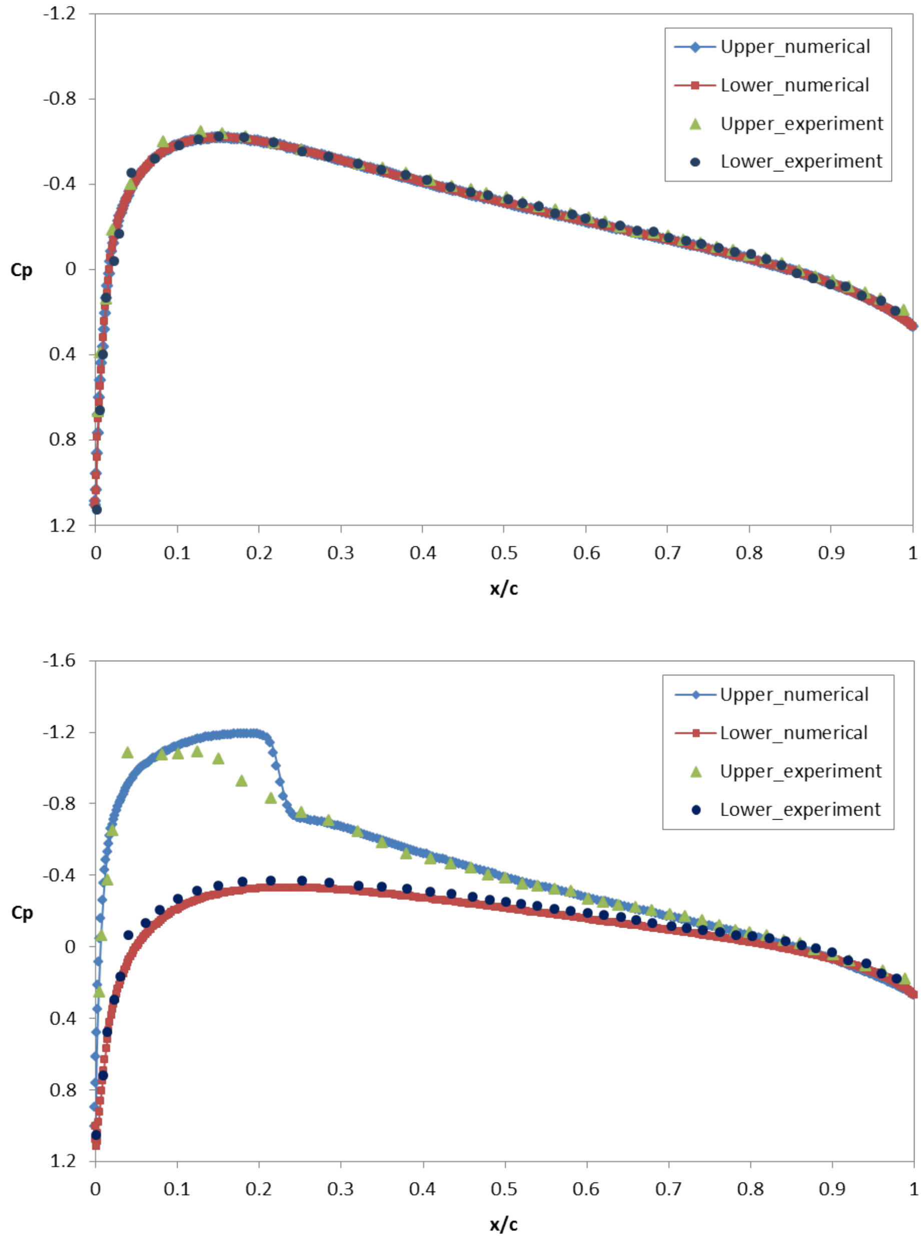

Figure 3.7 Case 1: Pressure coefficient distributions on NACA 0012 airfoil at $M = 0.7$, $R_c = 12 \times 10^6$, and $\alpha = 0$ and 2° respectively.

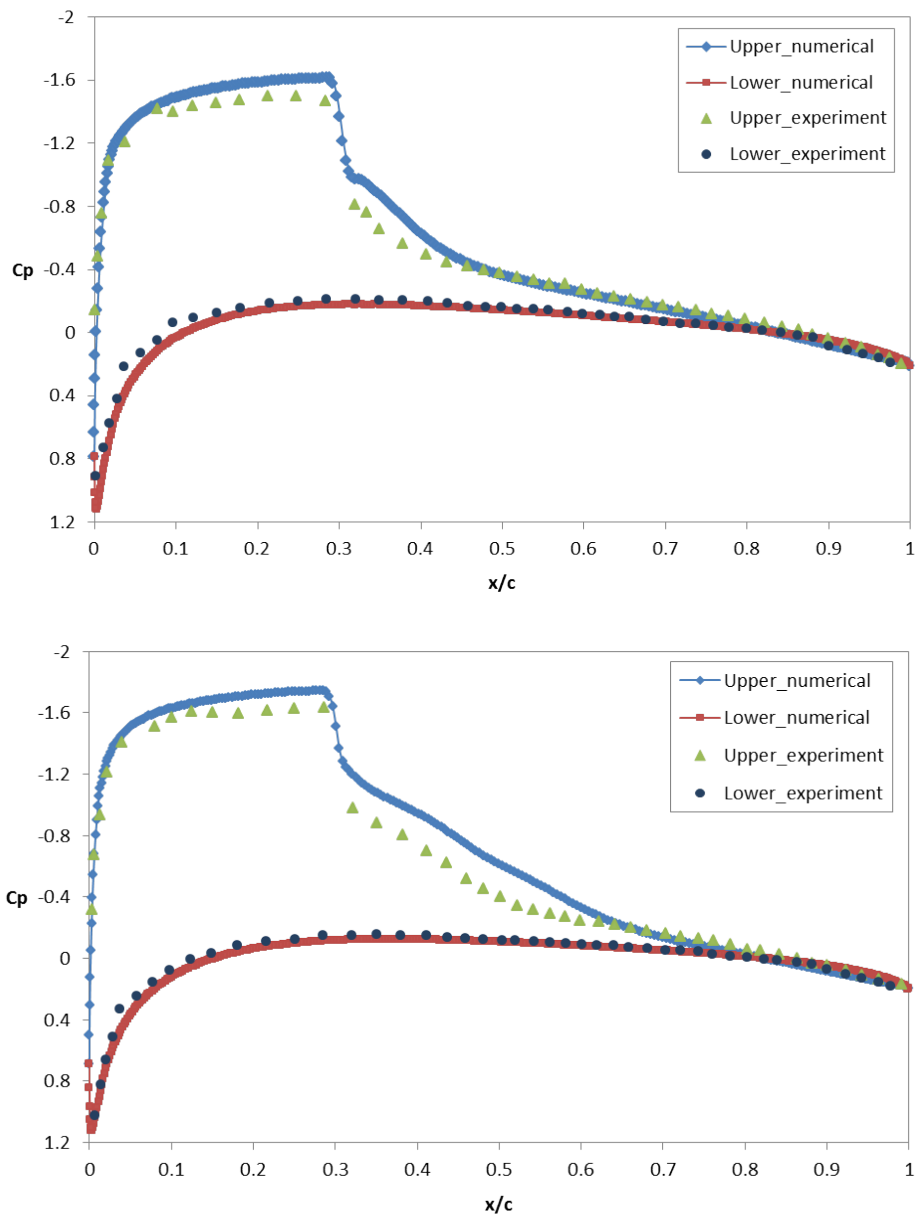

Figure 3.8 Case 1: Pressure coefficient distributions on NACA 0012 airfoil at $M = 0.7$, $R_c = 12 \times 10^6$, and $\alpha = 4$ and $5°$ respectively.

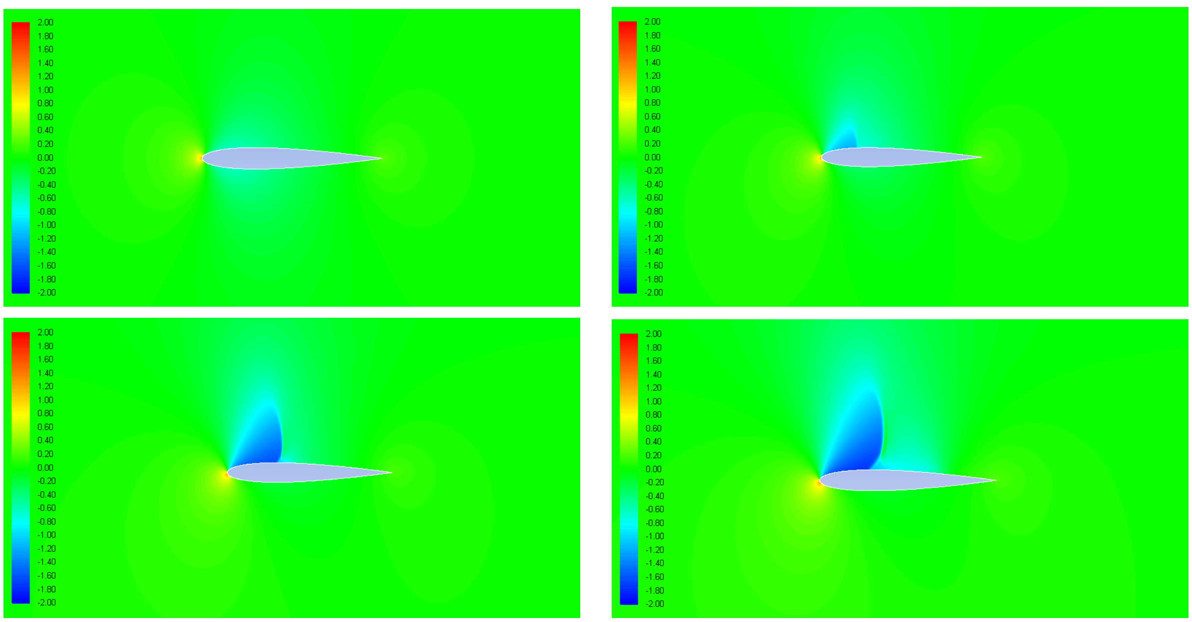

Figure 3.9 Case 1: Contour of pressure distributions on NACA 0012 airfoil at $M = 0.7$, $R_c = 12 \times 10^6$, and $\alpha = 0$, 2, 4, and 5° respectively.

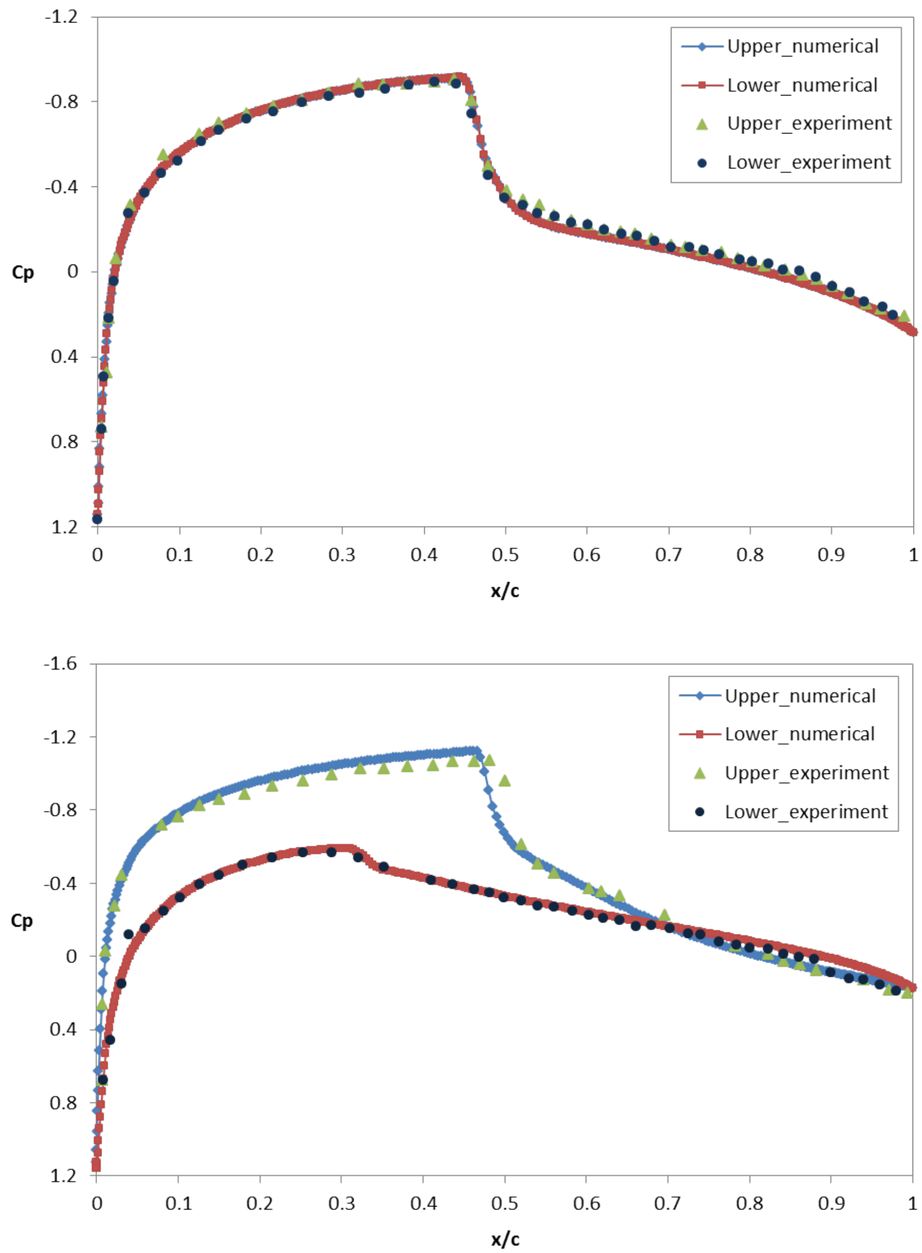

Figure 3.10 Case 1: Pressure coefficient distributions on NACA 0012 airfoil at $M = 0.8$, $R_c = 13 \times 10^6$, and $\alpha = 0$ and $2°$ respectively.

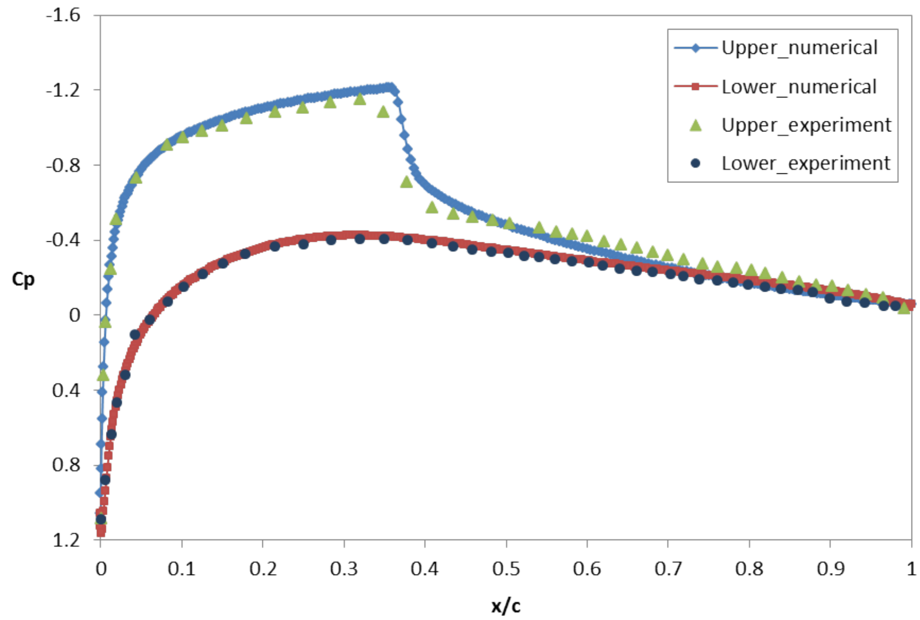

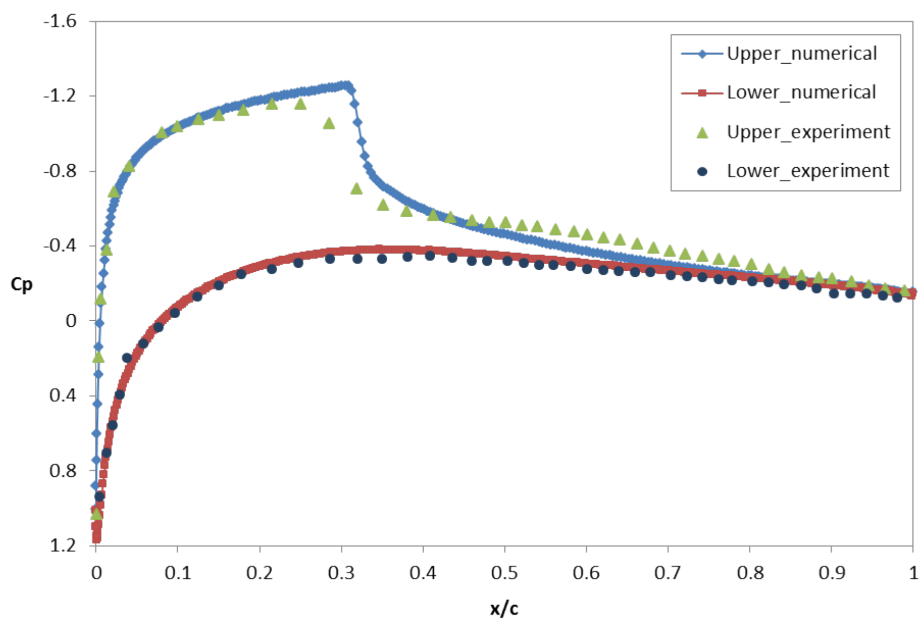

Figure 3.11 Case 1: Pressure coefficient distributions on NACA 0012 airfoil at $M = 0.8$, $R_c = 13 \times 10^6$, and $\alpha = 4$ and 5° respectively.

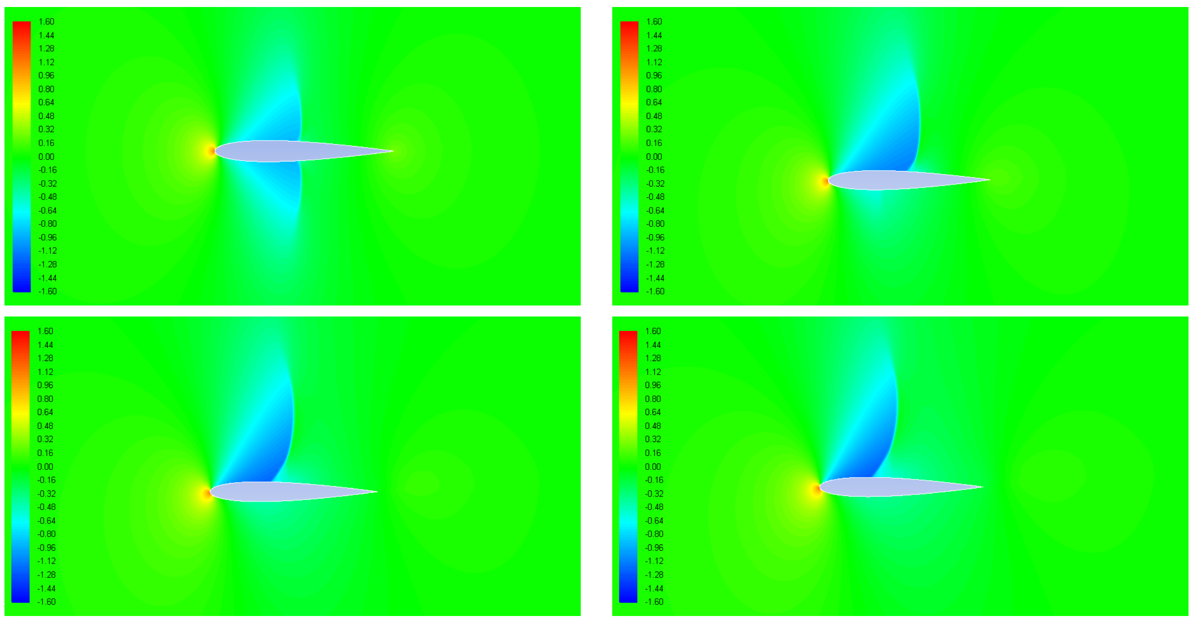

Figure 3.12 Case 1: Contour of pressure distributions on NACA 0012 airfoil at $M = 0.8$, $R_c = 13 \times 10^6$, and $\alpha = 0$, 2, 4, and 5° respectively.

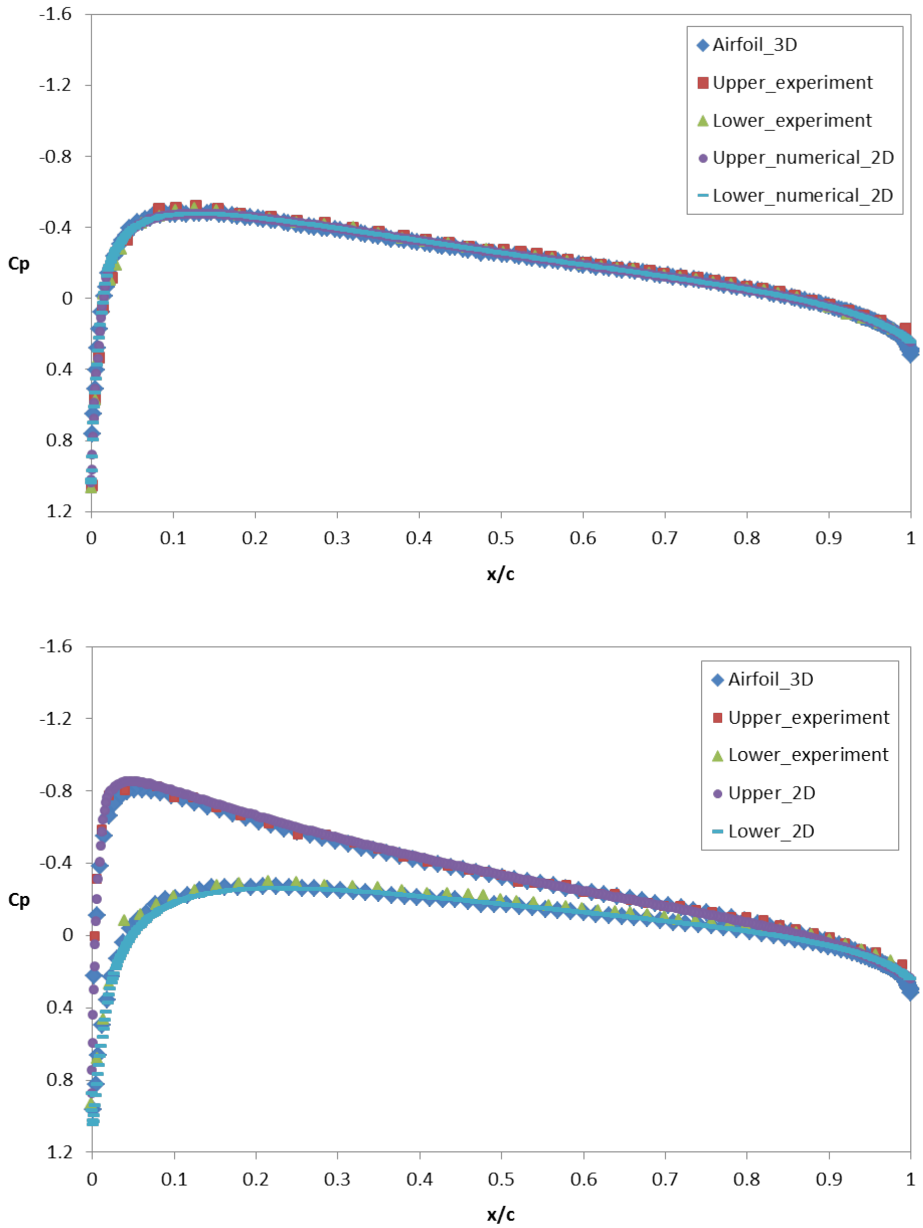

Figure 3.13 Case 2: Pressure coefficient distributions on NACA 0012 airfoil at $M = 0.5$, $R_c = 6 \times 10^6$, and $\alpha = 0$ and $2°$ respectively.

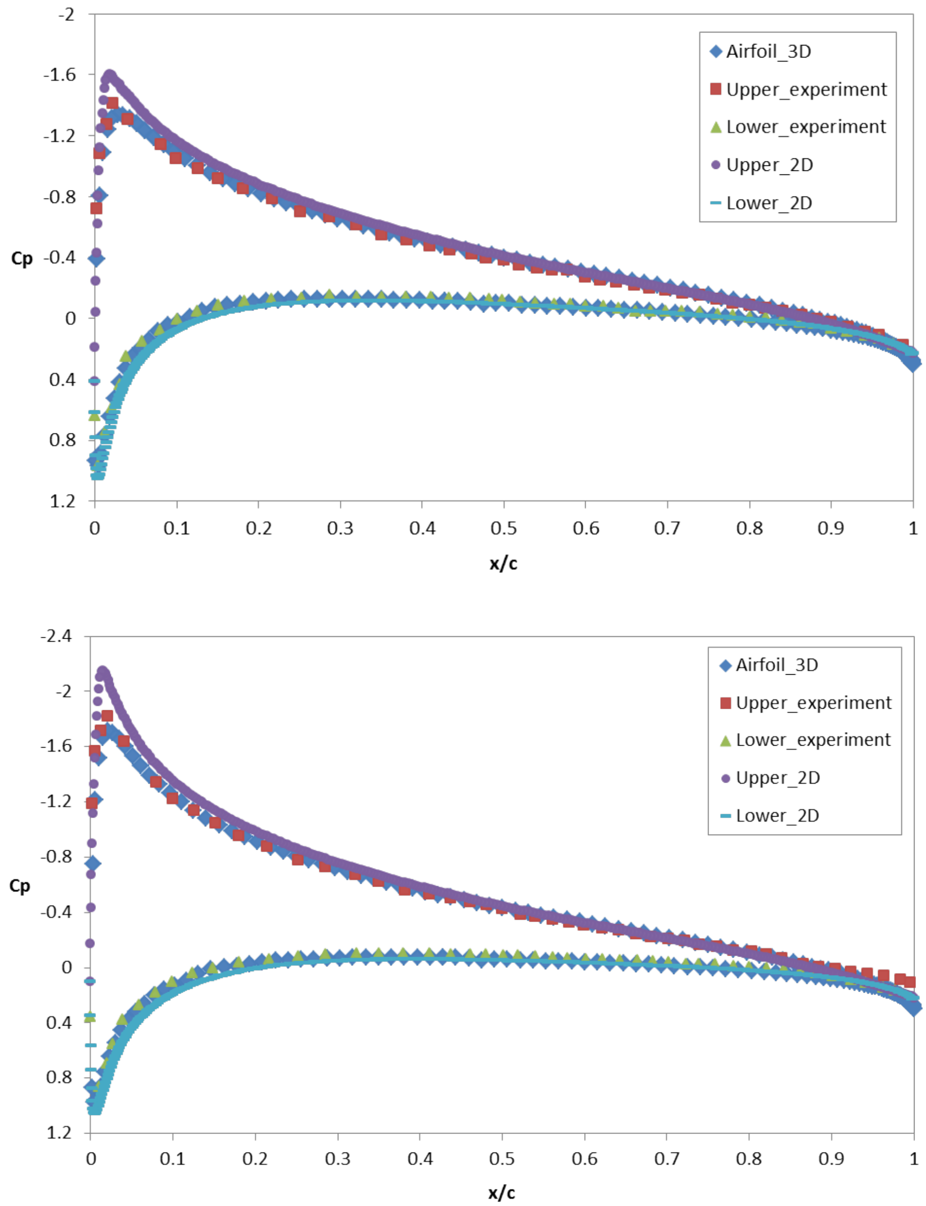

Figure 3.14 Case 2: Pressure coefficient distributions on NACA 0012 airfoil at $M = 0.5$, $R_c = 6 \times 10^6$, and $\alpha = 4$ and $5°$ respectively.

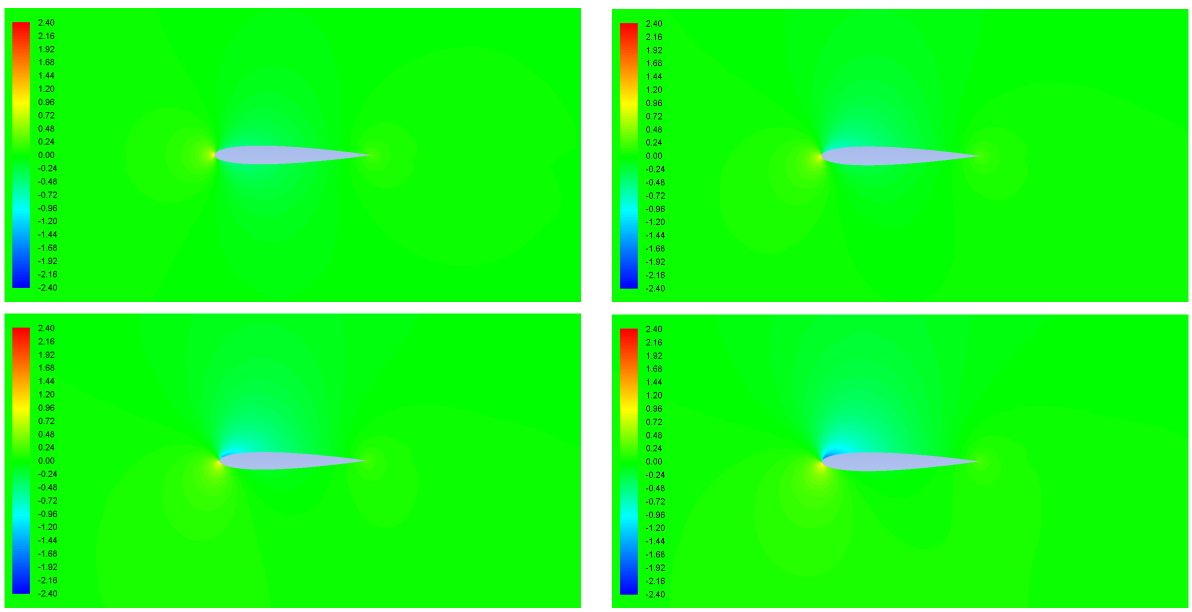

Figure 3.15 Case 2: Contour of pressure distributions on NACA 0012 airfoil at $M = 0.5$, $R_c = 6 \times 10^6$, and $\alpha = 0$, 2, 4, and 5° respectively.

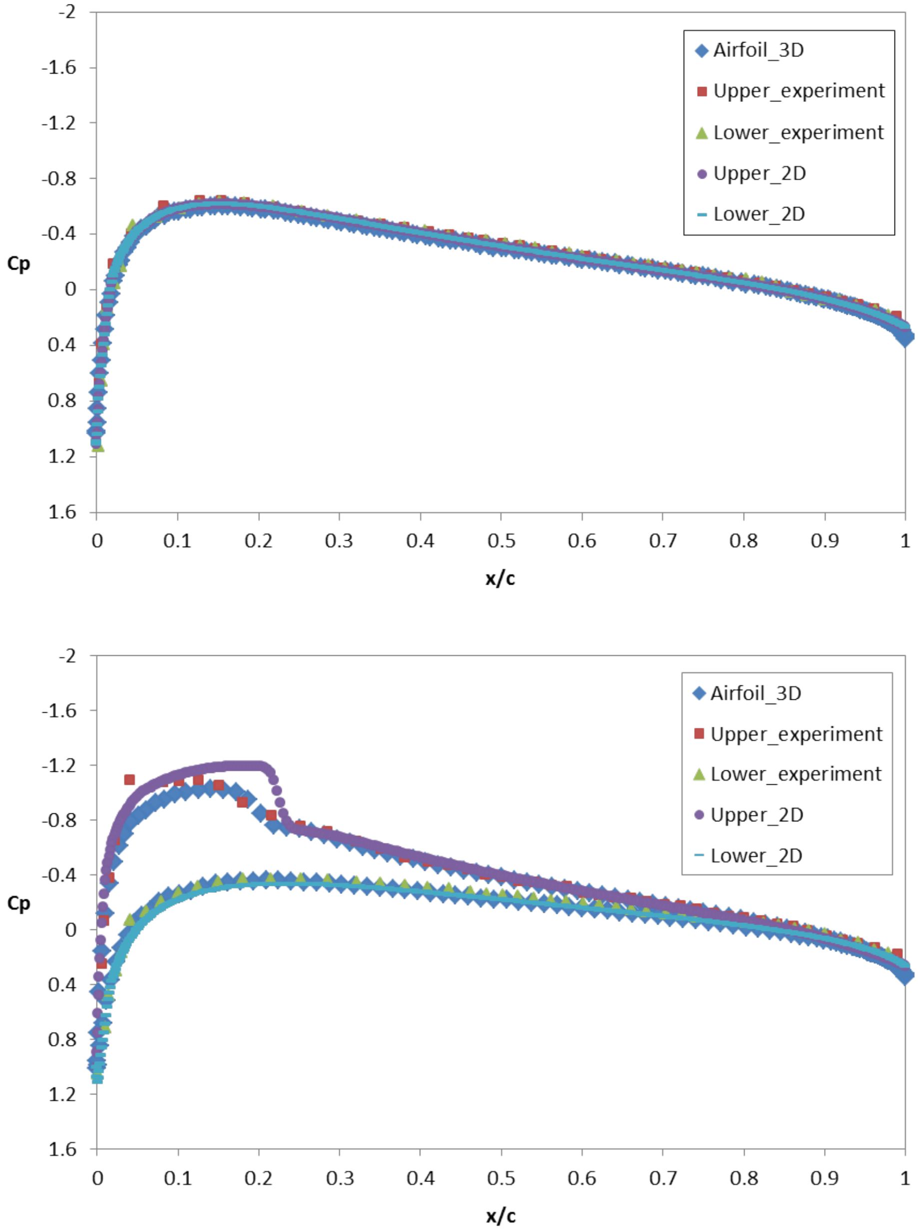

Figure 3.16 Case 2: Pressure coefficient distributions on NACA 0012 airfoil at $M = 0.7$, $R_c = 8 \times 10^6$, and $\alpha = 0$ and 2° respectively.

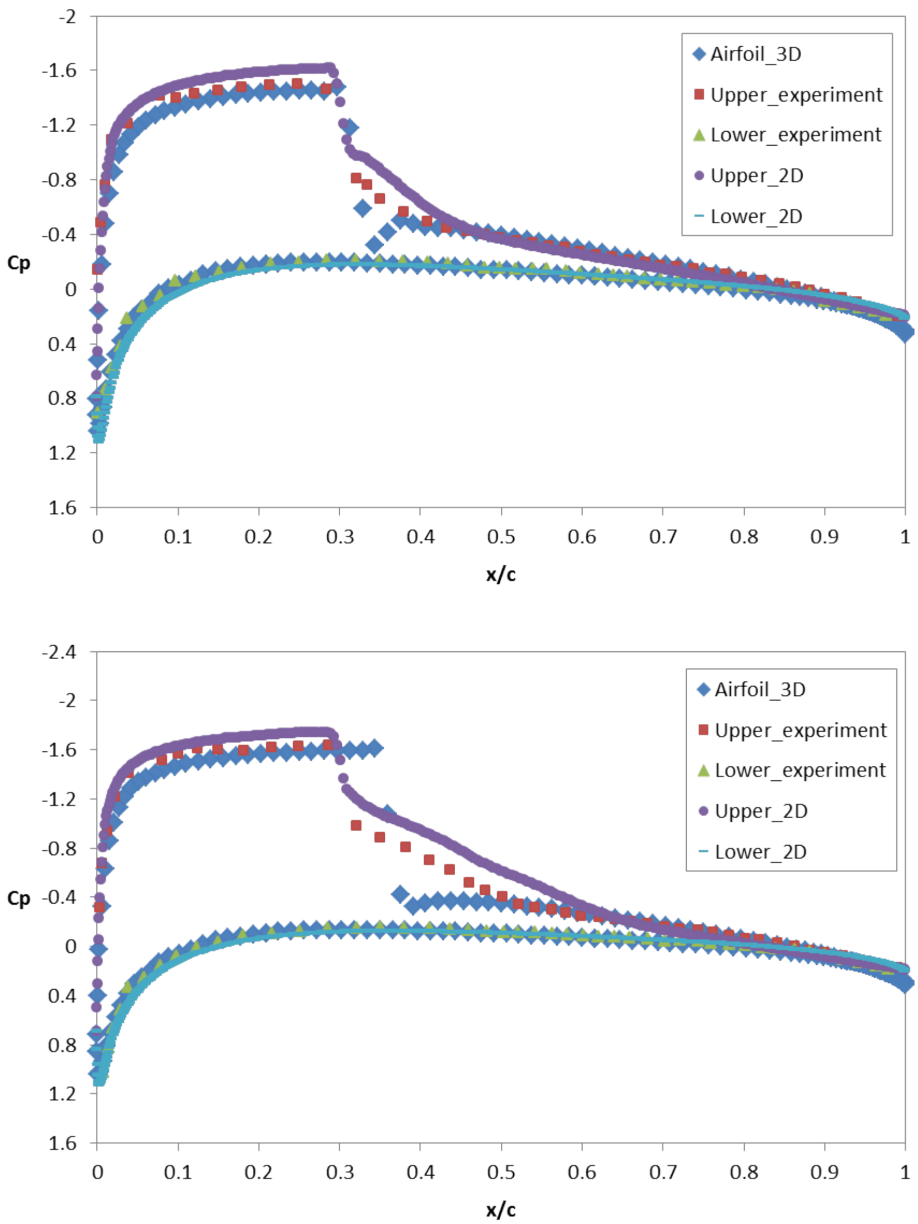

Figure 3.17 Case 2: Pressure coefficient distributions on NACA 0012 airfoil at $M = 0.7$, $R_c = 8 \times 10^6$, and $\alpha = 4$ and $5°$ respectively.

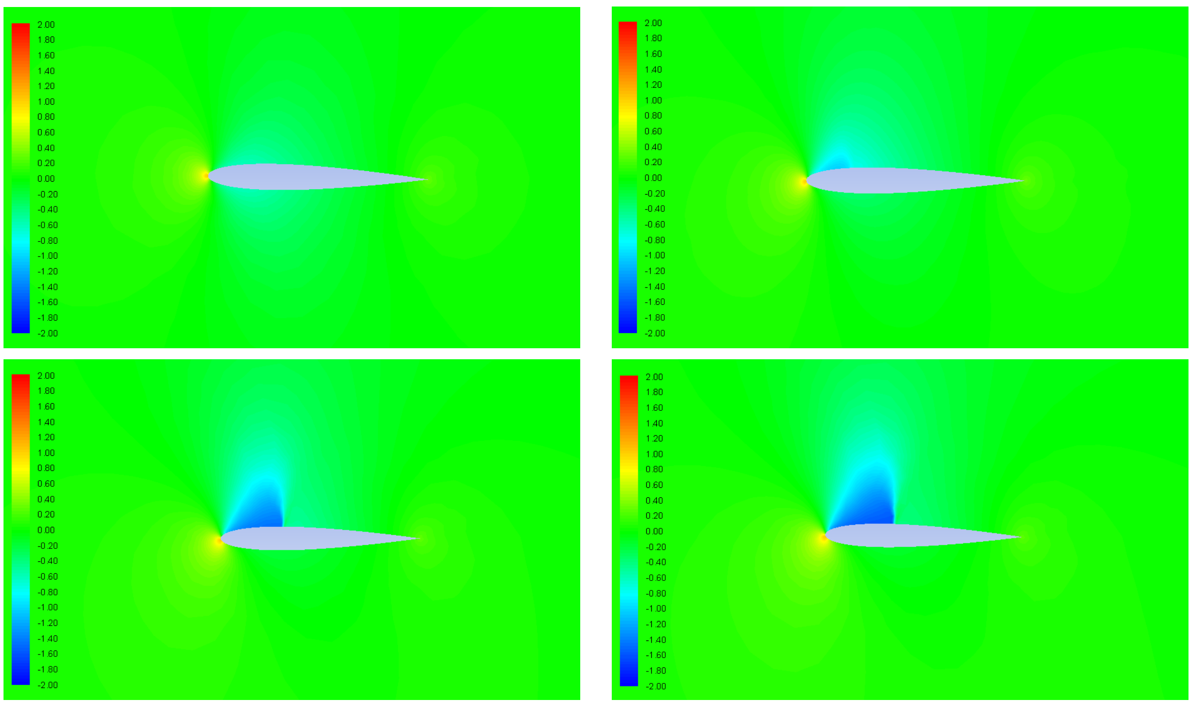

Figure 3.18 Case 2: Contour of pressure distributions on NACA 0012 airfoil at $M = 0.7$, $R_c = 8 \times 10^6$, and $\alpha = 0$, 2, 4, and 5° respectively.

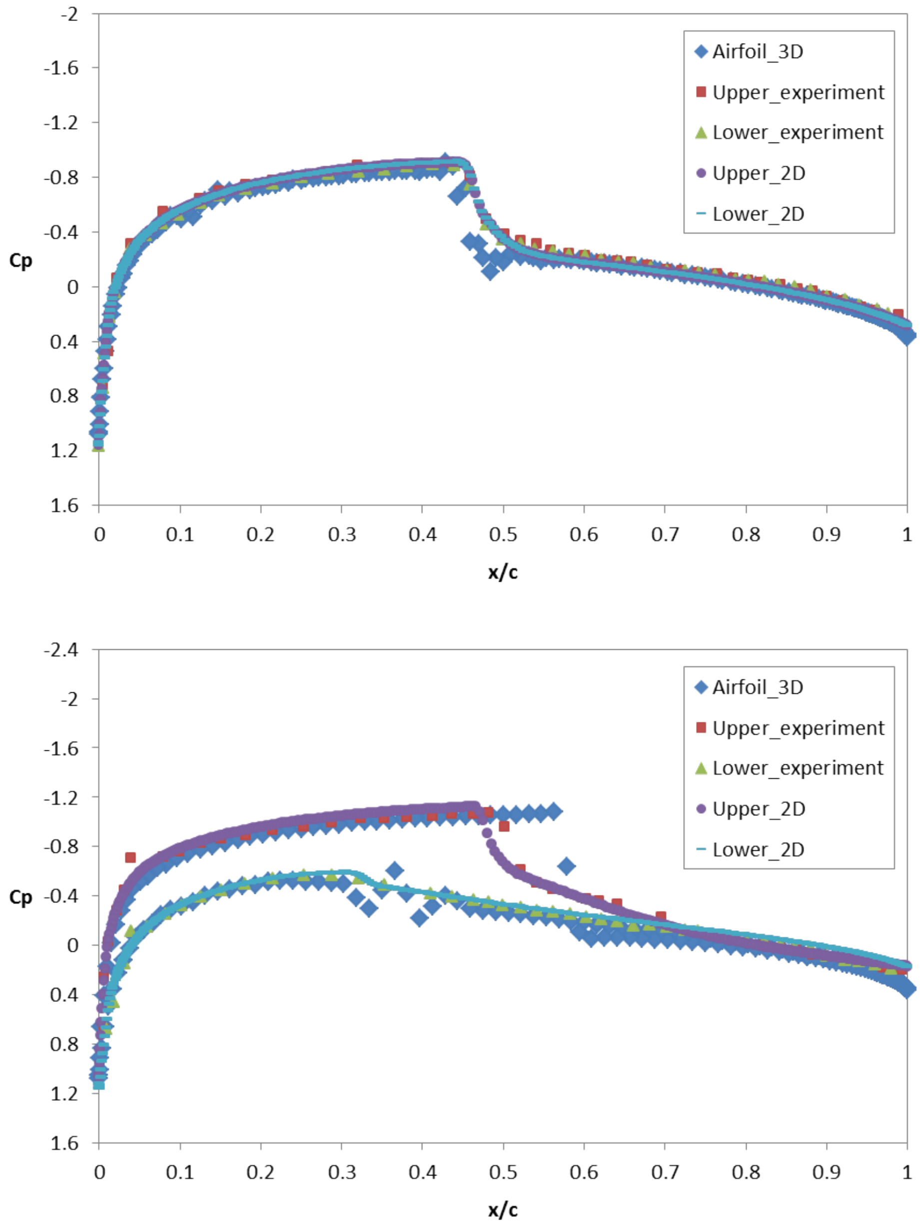

Figure 3.19 Case 2: Pressure coefficient distributions on NACA 0012 airfoil at $M = 0.8$, $R_c = 8 \times 10^6$, and $\alpha = 0$ and 2° respectively.

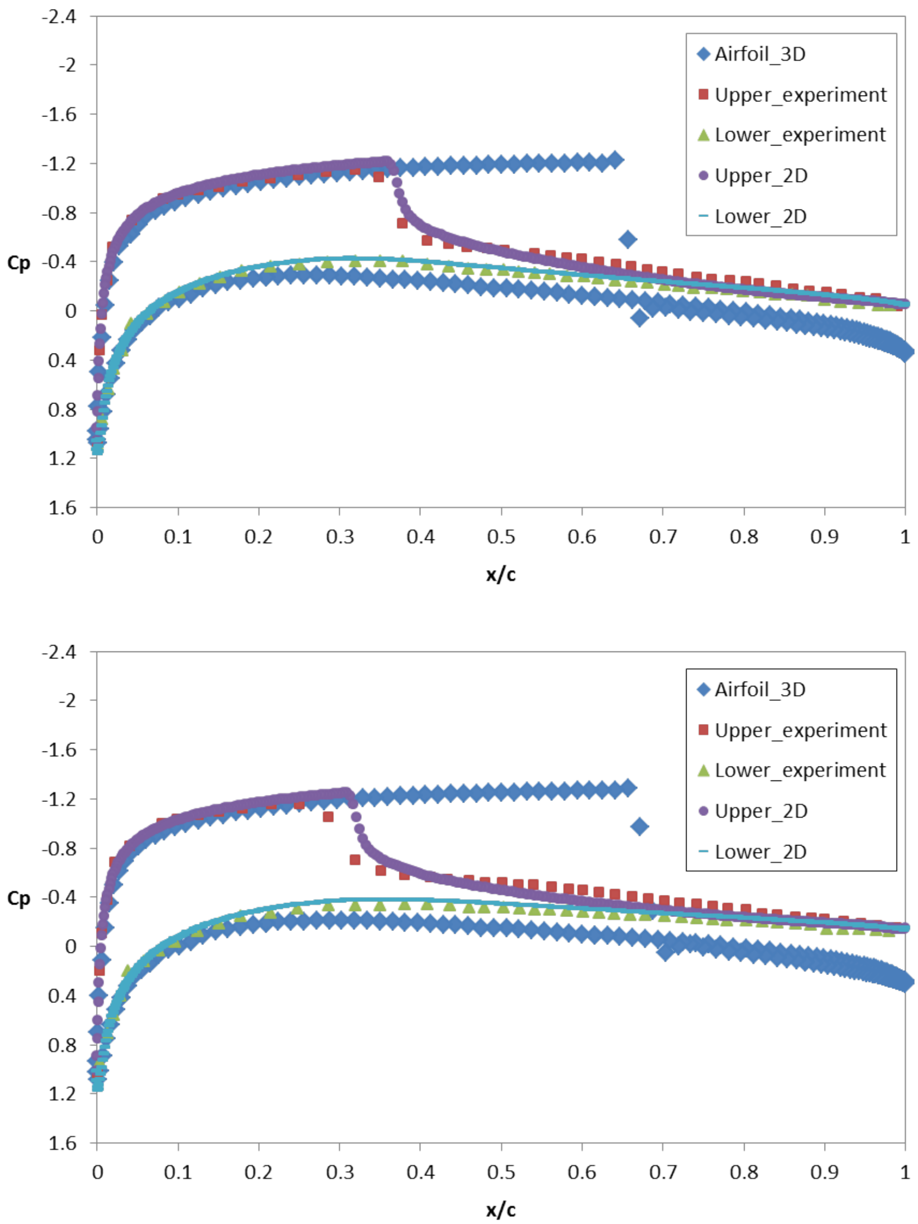

Figure 3.20 Case 2: Pressure coefficient distributions on NACA 0012 airfoil at $M = 0.8$, $R_c = 8 \times 10^6$, and $\alpha = 4$ and $5°$ respectively.

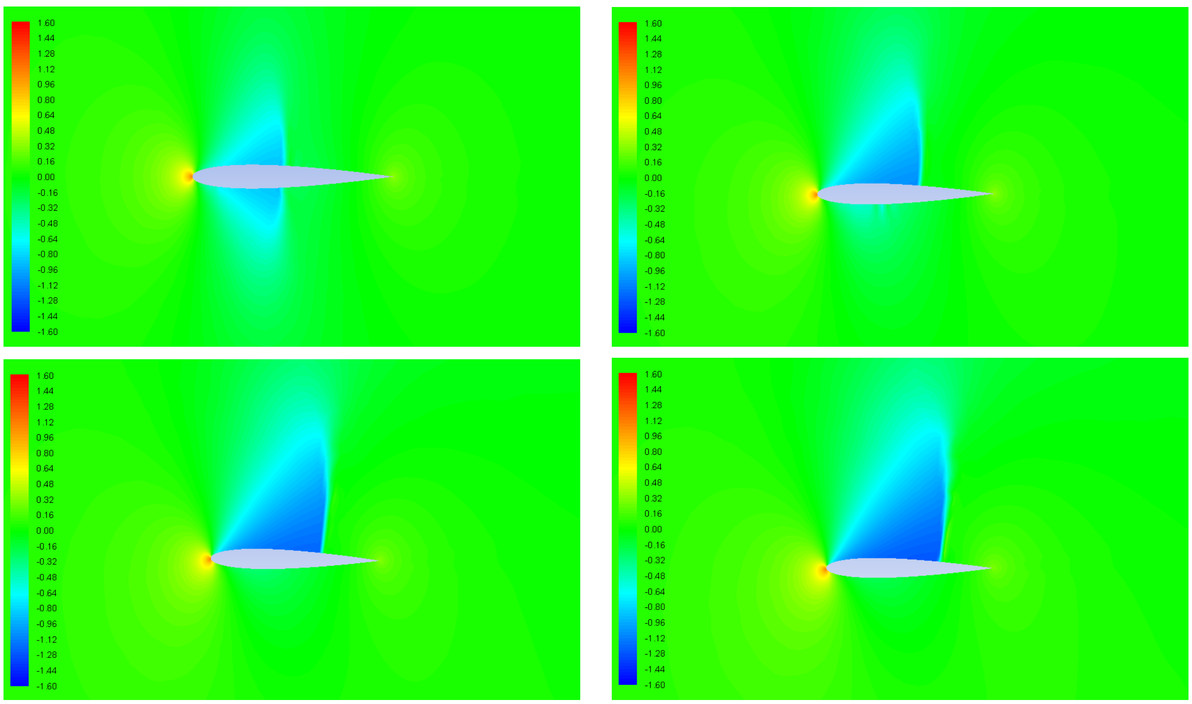

Figure 3.21 Case 2: Contour of pressure distributions on NACA 0012 airfoil at $M = 0.8$, $R_c = 8 \times 10^6$, and $\alpha = 0$, 2, 4, and 5° respectively.

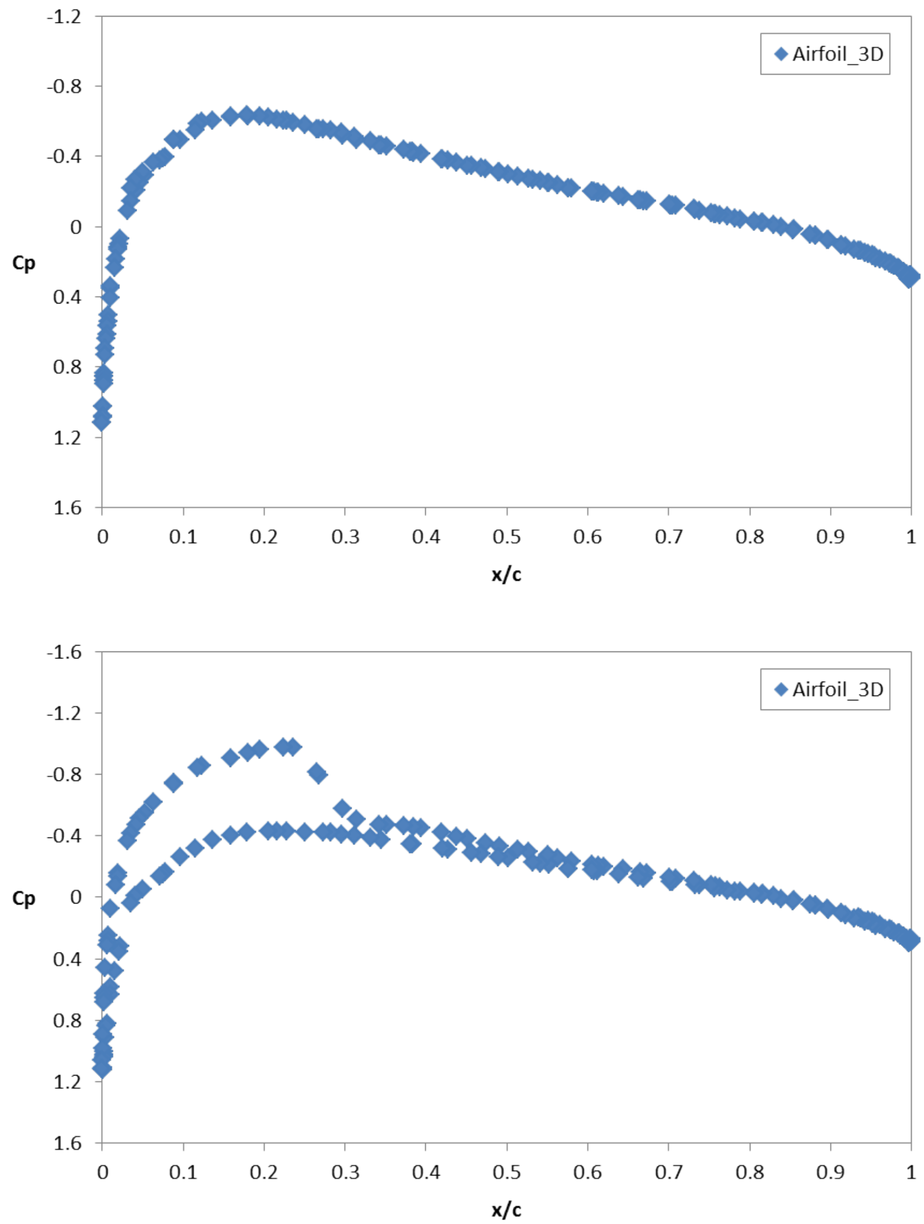

Figure 3.22 Case 3: Pressure coefficient distributions on NACA 0012 airfoil at $M = 0.75$, $R_c = 6 \times 10^5$, and $\alpha = 0$ and 2° respectively.

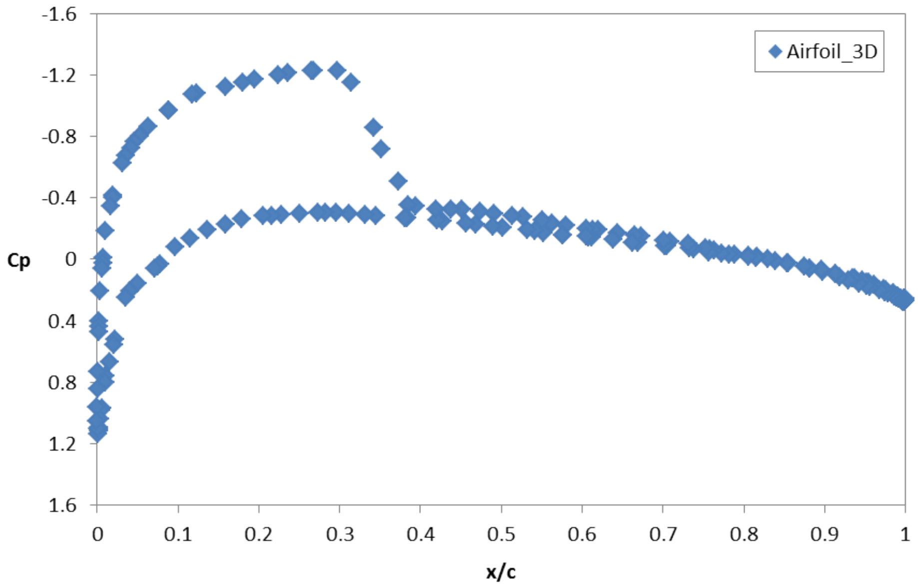

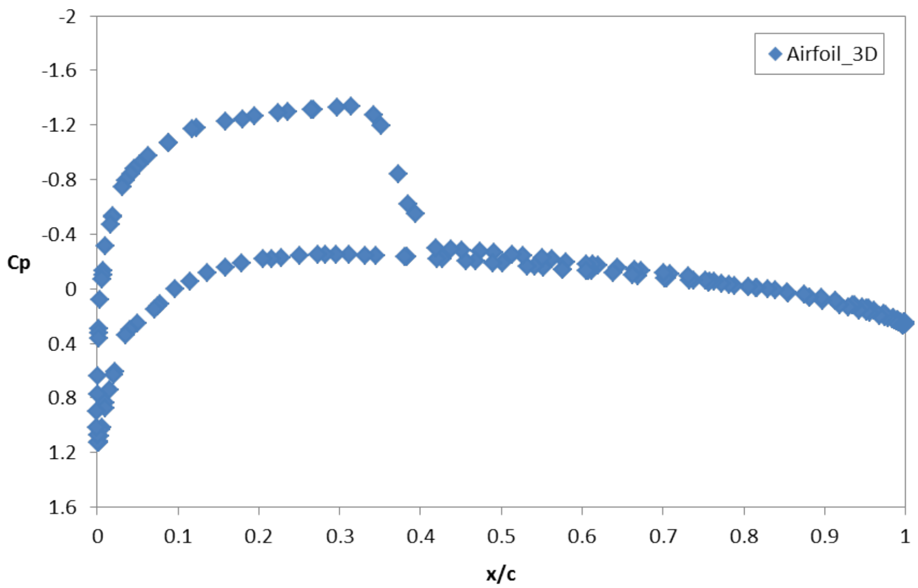

Figure 3.23 Case 3: Pressure coefficient distributions on NACA 0012 airfoil at $M = 0.75$, $R_c = 6 \times 10^5$, and $\alpha = 4$ and $5°$ respectively.

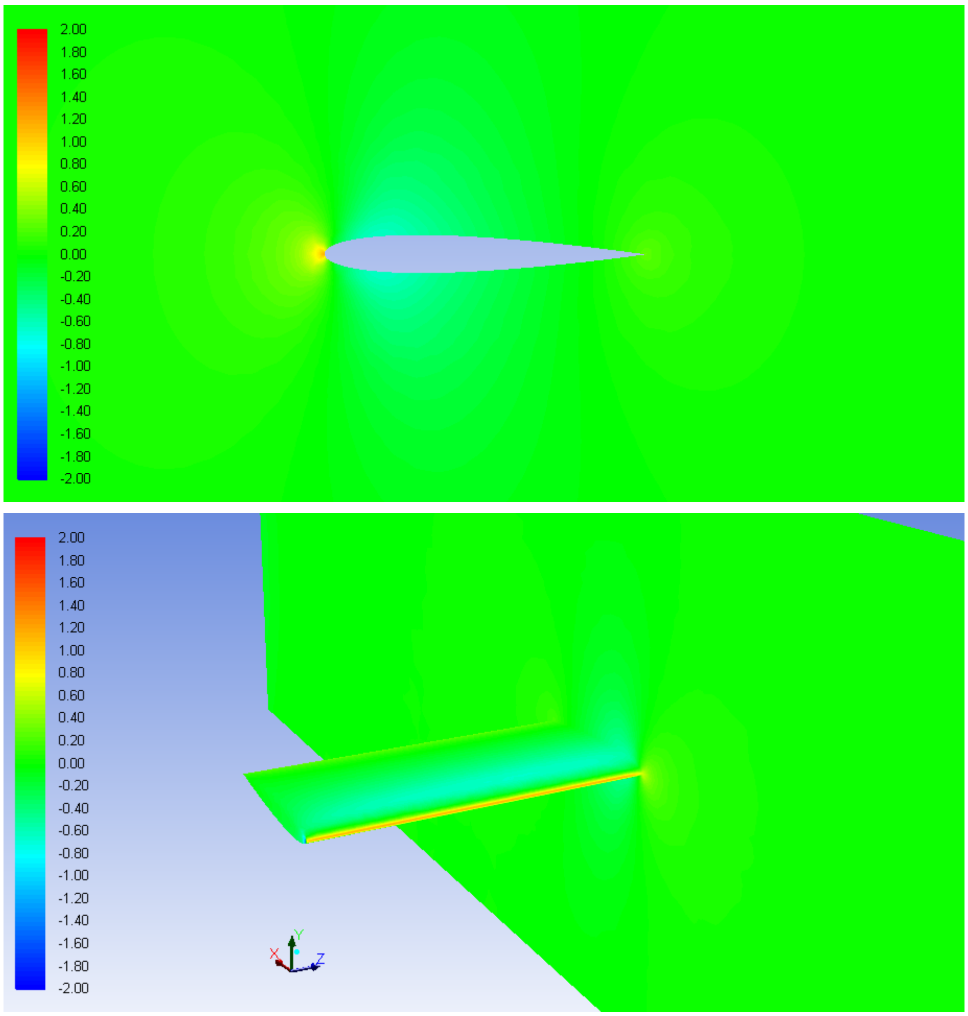

Figure 3.24 Case 3: Contour of pressure distributions on NACA 0012 airfoil at $M = 0.75$, $R_c = 6 \times 10^5$, and $\alpha = 0°$.

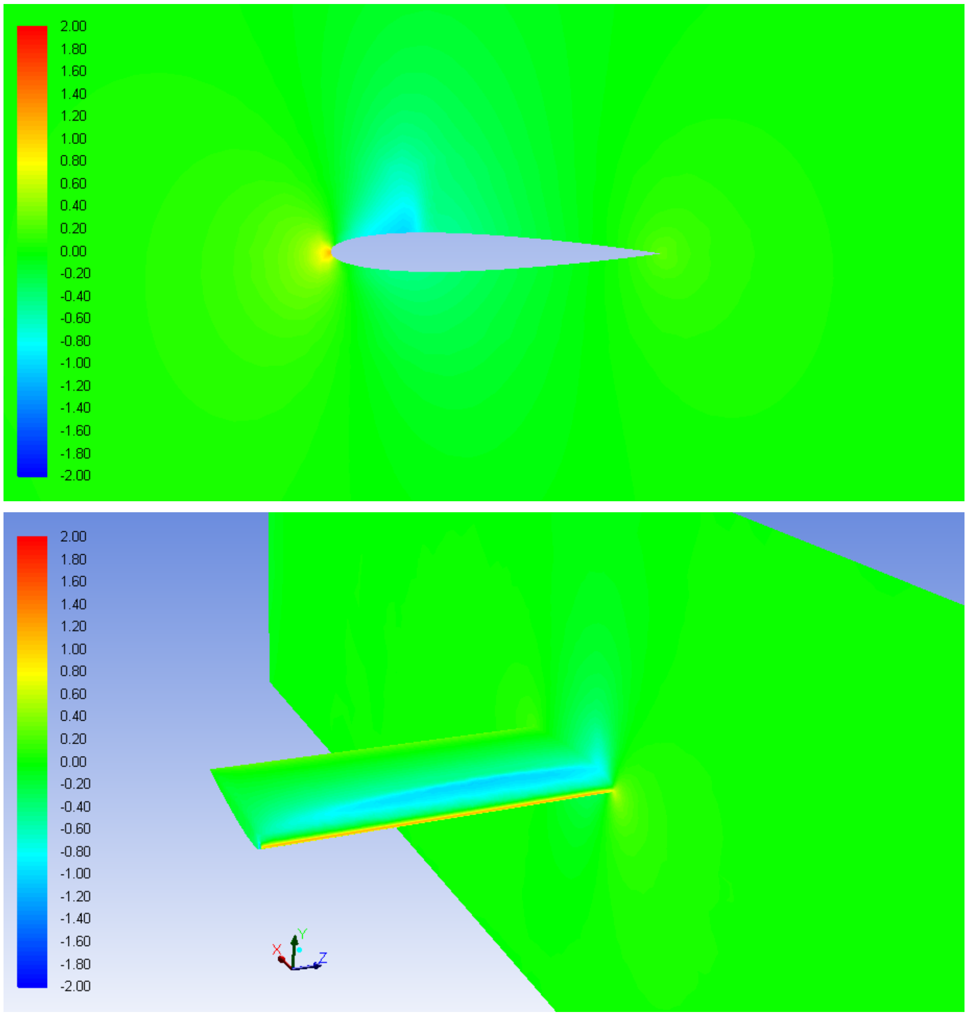

Figure 3.25 Case 3: Contour of pressure distributions on NACA 0012 airfoil at $M = 0.75$, $R_c = 6 \times 10^5$, and $\alpha = 2°$.

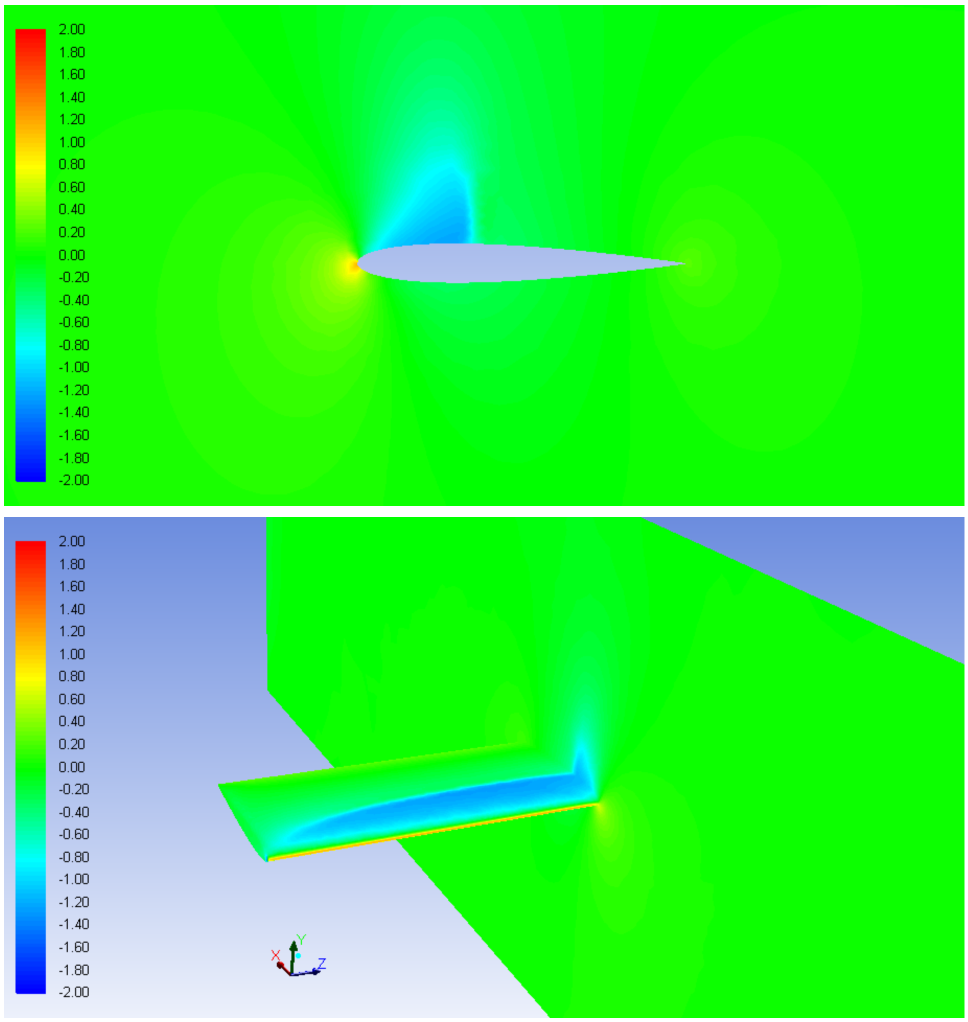

Figure 3.26 Case 3: Contour of pressure distributions on NACA 0012 airfoil at $M = 0.75$, $R_c = 6 \times 10^5$, and $\alpha = 4°$.

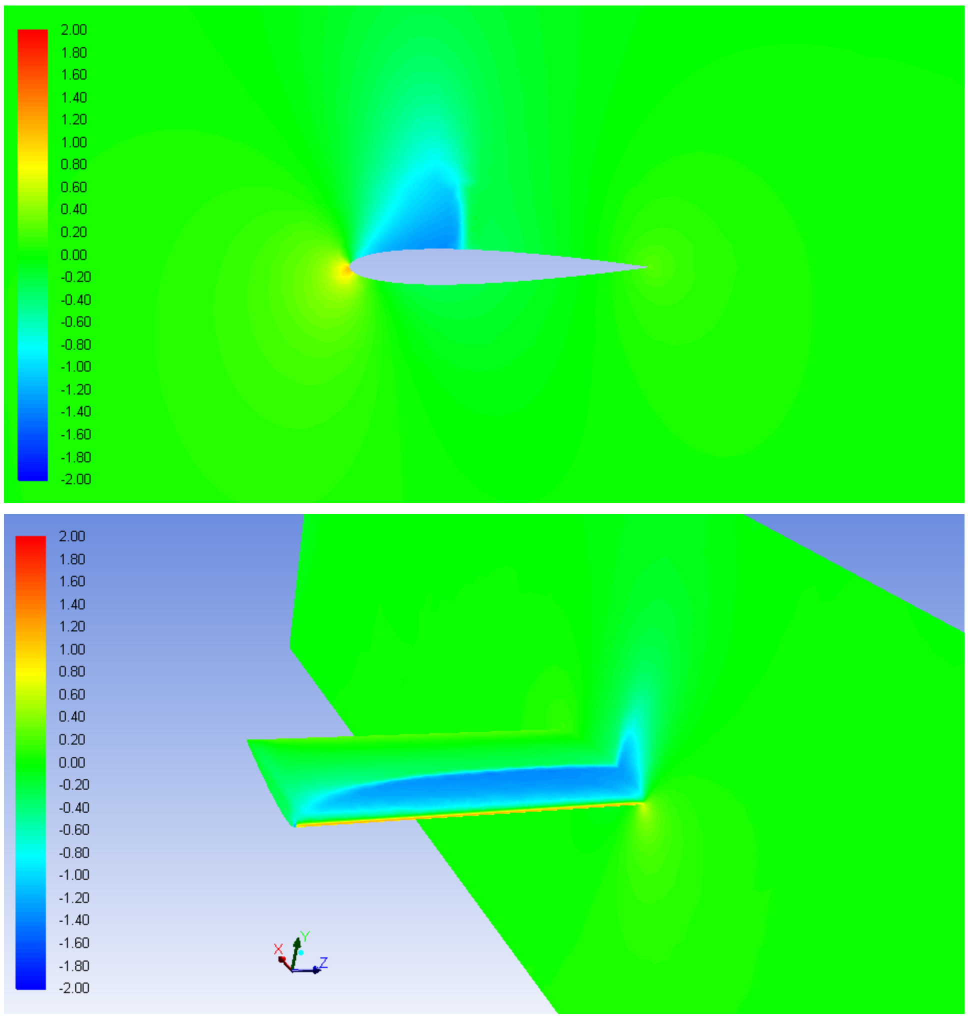

Figure 3.27 Case 3: Contour of pressure distributions on NACA 0012 airfoil at $M = 0.75$, $R_c = 6 \times 10^5$, and $\alpha = 5°$.

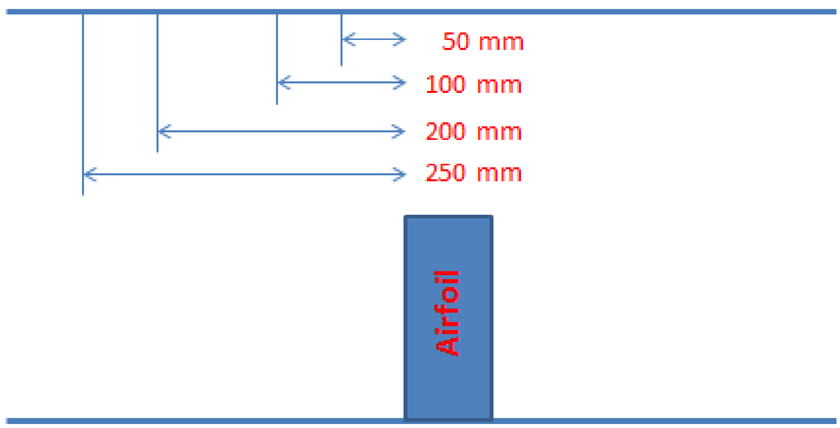

Figure 3.28 Case 3: Tunnel Wall Boundary-Layer Thickness layout.

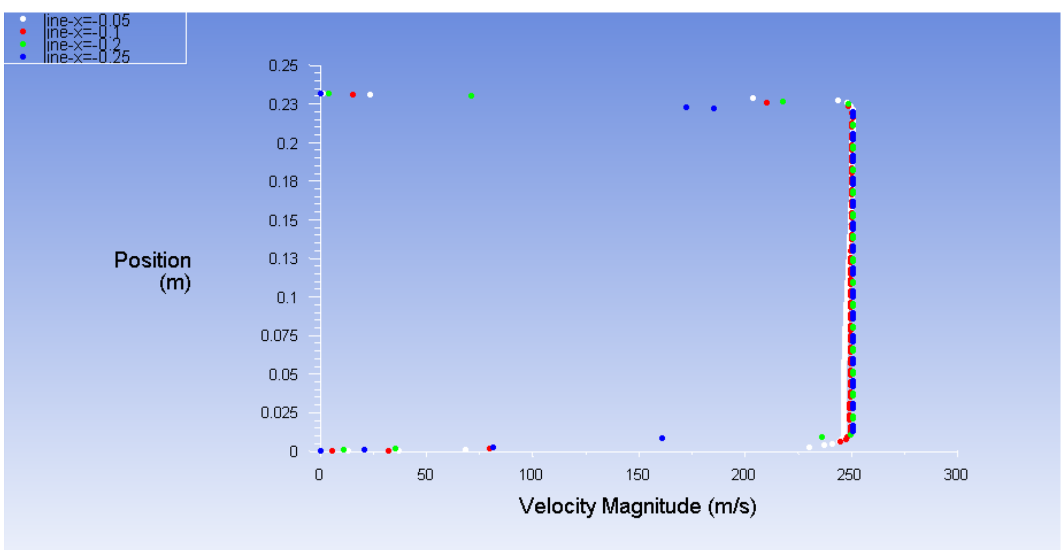

Figure 3.29 Case 3: Tunnel Wall Boundary-Layer Thickness at $M = 0.75$.

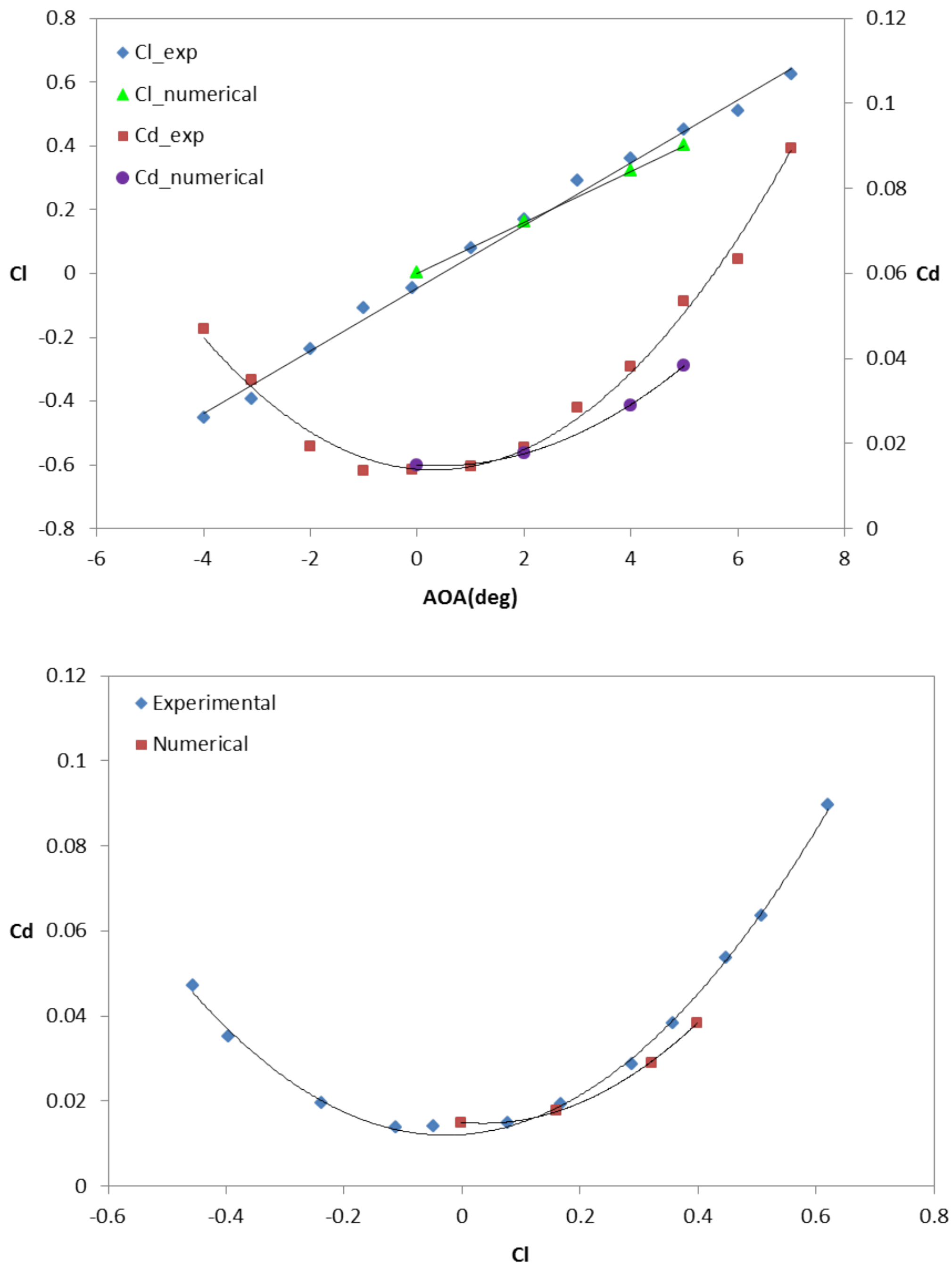

Figure 3.30 Comparison of lift and drag coefficient at $M = 0.75$ for a NACA 0012 airfoil wingtip.

CHAPTER 4

CONCLUSIONS AND FUTURE WORK

4.1 Conclusions

Numerical simulations are presented of the flow over a NACA 0012 wing in the transonic regime. The computations were performed in both two- and three-dimensions at various airfoil chord lengths and angles of attack. The three-dimensional simulations were conducted for a full- and a half-wing. Aerodynamic data such as pressure distributions, and lift and drag coefficients were obtained and compared with existing data. The comparisons showed discrepancies in regions of shock/boundary-layer interactions. Despite this, the overall lift and drag coefficients appeared to compare well with experimental results.

4.2 Future Work

Despite the difficulty in resolving regions with shock/boundary-layer interactions, the numerical simulations appeared to be suitable for studying transonic aerodynamics. Future work is to extend the study to more realistic supercritical airfoils and wings, including sweep.

REFERENCES

[1] X. Ren, Z. Zhao, and C. Gao, "Investigation of NACA 0012 airfoil periodic flows in a transonic wind tunnel," *AIAA Paper 2013-0791*, 2013.

[2] W. C. Selerowicz, "Prediction of transonic wind tunnel test section geometry – a numerical study," *The Archive of Mechanical Engineering*, vol. LVI, pp. 113–130, 2009.

[3] R. E. Mineck and P. M. Hartwich, "Effect of full-chord porosity on aerodynamic characteristics of the NACA 0012 airfoil," *NASA Technical Paper 3591*, 1996.

[4] M. G. Werling, Jr., J. E. Gutierrez, E. M. Braun, and F. K. Lu, "Force measurements on a NACA 0012 wingtip at Mach 0.75," *AIAA Paper 2013-1026*, 2013.

[5] D. C. Eleni, T. I. Athanasios, and M. P. Dionissios, "Evaluation of the turbulence models for the simulation of the flow over a National Advisory Committee for Aeronautics (NACA) 0012 airfoil," *Journal of Mechanical Engineering Research*, vol. 4(3), pp. 100–111, 2012.

BIOGRAPHICAL STATEMENT

Suparat Chanrith was born in Phitsanulok, Thailand, in 1984. He was given an opportunity to study at the Royal Thai Air Force Academy and completed his B.S. in Aeronautical Engineering in 2006. He worked as an engine maintenance engineer of the Engine Maintenance Division, Directorate of Aeronautical Engineering. He was interested in the sophistication of the flow passing through the turbine section of an aircraft's engine, so he made a decision to pursue his masters degree in Aerospace Engineering at the University of Texas at Arlington.